ELSEVIER

Contents lists available at ScienceDirect

Biomaterials

journal homepage: www.elsevier.com/locate/biomaterials





Zn0.8Li0.1Sr—a biodegradable metal with high mechanical strength comparable to pure Ti for the treatment of osteoporotic bone fractures: *In vitro* and *in vivo* studies

Zechuan Zhang ^{a,1}, Bo Jia ^{b,c,1}, Hongtao Yang ^{a,d}, Yu Han ^b, Qiang Wu ^b, Kerong Dai ^{b,**}, Yufeng Zheng ^{a,*}

- ^a School of Materials Science and Engineering, Peking University, Beijing, 100871, China
- b Department of Orthopaedic Surgery, Shanghai Key Laboratory of Orthopaedic Implants, Shanghai Ninth People's Hospital, Shanghai Jiao Tong University, School of Medicine, Shanghai, 200011, China
- ^c Department of Orthopaedics, Shanghai General Hospital, Shanghai Jiao Tong University School of Medicine, Shanghai, 200080, China
- ^d School of Medical Science and Engineering, Beihang University, Beijing, 100191, China

ARTICLE INFO

Keywords:
ZnLiSr alloys
Biodegradable metals
Strength-ductility balance
Osteoporotic bone fractures
Osteogenesis
OVX rat Model

ABSTRACT

The first *in vivo* investigation of Zn-based biodegradable metal aiming to treat osteoporotic bone fractures, a soaring threat to human health, is reported in this paper. Among the newly developed biodegradable metal system (ZnLiSr), Zn0.8Li0.1Sr exhibits excellent comprehensive mechanical properties, with an ultimate tensile strength (524.33 \pm 18.01 MPa) comparable to pure Ti (the gold standard for orthopaedic implants), and a strength-ductility balance over 10 GPa%. The *in vitro* degradation tests using simulated body fluid (SBF) shows that Zn0.8Li0.1Sr manifests a uniform degradation morphology and smaller corrosion pits, with a degradation rate of $10.13 \pm 1.52~\mu m$ year $^{-1}$. Real-time PCR and western blotting illustrated that Zn0.8Li0.1Sr successfully stimulated the expression of critical osteogenesis-related *genes* (ALP, COL-1, OCN and Runx-2) and proteins. Twenty-four weeks' *in vivo* implantations within ovariectomized (OVX) rats were conducted to evaluate the osteoporotic-bone-fracture-treating effects of Zn0.8Li0.1Sr, with pure Ti as control group. Micro-CT, histological and immunohistochemical evaluations all revealed that Zn0.8Li0.1Sr possesses a similar biosafety level to, while significantly superior osteogenesis-inducing and osteoporotic-bone-fracture-treating effects than pure Ti. ZnLiSr biodegradable alloys manifest excellent comprehensive mechanical properties, good biosafety and osteoporotic-bone-fracture-treating effects, which would provide preferable choices for future medical applications, especially in load-bearing positions.

1. Introduction

Osteoporosis, one of the most common skeletal diseases [1], is growing into a huge problem with the global population aging becoming increasingly grim. It is anticipated that by 2050, the elderly people (65 years old or over), for the first time in human history, would outnumber the adolescents and youth (15–24 years old) [2]. Inevitably, more and more medical resources would be put into treating diseases typically related with an older population, including osteoporosis and its successive bone fractures. Some kinds of osteoporotic bone fractures, such

as pelvic and femoral ones, are linked with a higher morbidity and mortality, which would severely affect the patients' life quality, usually depriving their ability to live independently and leaving their mental health to a very stressful status [3,4].

For the treatment of bone fractures, metallic biomaterials are widely used [5]. Nonetheless, traditional non-degradable metals, like titanium and stainless steel, have displayed insurmountable disadvantages, such as inducing chronic inflammatory reactions [6], demanding a secondary surgery to be removed after the treatment, etc. [7]. During the bone healing process, a typical problem well known as stress-shielding

 $^{^{\}ast}$ Corresponding author.

^{**} Co-Corresponding author. Department of Orthopaedics, Ninth People's Hospital, Shanghai Jiao Tong University, School of Medicine, 639 Zhizaoju Road, Shanghai, 200011, China.

E-mail addresses: krdai@163.com (K. Dai), yfzheng@pku.edu.cn (Y. Zheng).

 $^{^{1}\,}$ These authors contributed equally to this work.

frequently emerges due to the excessive load-carrying by the implants, which would deprive the bone of the stress necessary to restore its strength, entailing a high risk of re-fractures in later days [8]. Hence, an ideal metallic biomaterial for orthopaedic treatments should be biodegradable, which means it should not only completely dissolve without residues as soon as the tissue heals [5], but also gradually reduce its mechanical strength, transferring enough load to the bone to help it regain strength [8]. This desire for ideal biodegradable metals in orthopaedics have already intrigued many researchers. Up to now, there have been mainly three alloy systems being investigated as biodegradable metals, including the Fe alloy system, Mg alloy system and Zn alloy system. Among these systems, Fe alloys' intrinsic ferromagnetic properties render them unsuitable to cooperate with MRI, a commonly used inspecting medical means. In addition, their over-slow degradation rates and over-high Young's modulus cannot satisfy the clinical requirements in orthopaedics [5,9]. Mg alloys, on the other hand, cannot provide high-enough strength for load-bearing usages. Besides, during Mg alloys' degradation, there would inevitably produce hydrogen bubbles which may retard the normal healing process of tissue [10,11].

Recently, Zn alloys have become the star of biodegradable materials researches. Zn is an indispensable element in bone metabolism [12], and Zn alloys don't exhibit the aforementioned disadvantages of Mg alloys or Fe alloys. However, the low mechanical properties, unsatisfactory degrading behaviors and cytotoxicity of pure Zn still cannot fulfill the standards of ideal biodegradable metals [13]. Consequently, it becomes necessary to improve the Zn alloys' performances [14]. In previous studies, alloying elements including Li [15–18], Mg [11,19,20], Sr [19], Ca [19], Mn [21–23], Fe [24], Cu [25,26] and Ag [27,28], have been introduced into developing Zn alloys, among which element Li have brought the most significant improvement in Zn alloys' mechanical behaviors [17], laying a good foundation for further optimization.

To improve ZnLi alloys' performances, element Sr was introduced into the alloy system. Sr is an essential element participating in the regulations of bone remodeling process [29]. Drugs containing Sr, such as strontium ranelate, have proved effective in preventing and treating osteoporotic bone fractures [30]. Sr element has been widely used in modifying biomaterials, such as 45S5 bioglass® [31], hydroxyapatite (HA) [32], and titanium implants [33]. Sr is also an important alloying element used in the development of biodegradable metals. Previous researches, such as MgSr [34–36] and ZnSr alloys [19], have already shown that Sr could improve the mechanical properties, biosafety as well as adjust the alloys' degrading properties. Therefore, Sr becomes a reasonable choice when a third alloying element was sought for the ZnLi alloys.

In this work, a novel ZnLiSr alloy system was developed through micro-alloy method. The target biodegradable metal should both satisfy the clinical requirements in practice and help to treat osteoporotic bone fractures. The microstructures, mechanical properties and degradation properties of ZnLiSr alloys were carefully studied. Then experiments evaluating the alloys' biosafety both in vitro and in vivo were conducted. Through researches in vitro, ZnLiSr alloys exhibited superb comprehensive mechanical properties with a strength-ductility balance over 10 GPa%, and excellent physiological properties compared to the control groups (pure Zn and Zn0.8Li). Through researches in vivo, Zn0.8Li0.1Sr manifested significant osteogenesis-inducing and osteoporotic-bonefracture-treating effects compared to pure Ti, which is recognized as the gold standard for orthopaedic applications nowadays. In a word, Zn0.8Li0.1Sr alloy exhibits promising potentials to serve for patients with osteoporotic bone fractures, supplying preferable choices for medical applications in the future.

2. Materials and methods

2.1. Materials preparation

The ZnLiSr alloy system and control groups (pure Zn and Zn0.8Li)

were prepared using high-purity Zn(99.99%), Li(99.95%) and Sr (99.99%) metals according to each alloy's composition, as listed in Table 1. Firstly, the pure metals were melt at 540 °C. Then the mixture was cast into cylindrical shape. All the as-cast alloys were prepared in Hunan Rare Earth Metal Material Research Institute. Then the as-cast alloys were extruded into bars at a temperature of 210 °C with an extrusion ratio of 16:1. Then different specimens were wire-cut from the extruded bars according to different tests' requirement. Disk-like specimens used for microstructure analyses, *in vitro* degradation tests, electrochemical tests and *in vitro* biosafety tests were cut perpendicular to the extrusion direction, with a dimension of Φ 10 × 2 mm³. All specimens were mechanically polished, rinsed by ethanol and acetone, and dried in the air.

2.2. Microstructural characterization

The metallographic structures of the alloys were obtained using an optical microscope (BX51 M, Olympus). Before the observation, samples were polished through a series of sandpapers (400#, 1200#, 2000#, 5000# and 7000#) to obtain smooth surfaces without scratch. Then the samples were etched in 4% natal, rinsed with ethanol, and dried in the air. Both as-cast and as-extruded samples were observed. The phase compositions of the as-extruded samples were detected using an X-ray diffractometer (XRD DMAX 240, Rigaku) equipped with Cu K α radiation, at a rate of $4^\circ/min$.

2.3. Mechanical tests

Specimens for tensile tests were prepared according to ASTM-E8-04a. The tensile tests were conducted on a universal material testing machine (Instron 5969, USA). The displacement rate was set at 1×10^{-4} s⁻¹. The yield strength (YS), ultimate tensile strength (UTS) as well as ductility (δ , calculated as the elongation of the sample after tensile test) were measured. Vickers hardness tests were conducted via a microhardness tester (SHIMADZUHMV-2t), with a loading force of 0.1 kN and a duration of 15s.

2.4. In vitro degradation tests

2.4.1. Electrochemical tests

A three-electrode cell system was employed for the electrochemical test, with a platinum electrode as counter electrode (CE), a saturated calomel electrode (SCE) as reference electrode (RE), and samples being tested as working electrodes (WE). Simulated body fluid (SBF) solution was chosen as the filling solution in the cell system. The composition of SBF [37,38] is: NaCl $8.035~g~L^{-1}, NaHCO_3~0.355~g~L^{-1}, KCl~0.25~g~L^{-1}, K_2HPO_4\cdot 3H_2O~0.231~g~L^{-1}, MgCl_2\cdot 6H_2O~0.311~g~L^{-1}, HCl~(36–38\%)~39~mL~L^{-1}, CaCl_2~0.292~g~L^{-1}, Na_2SO_4~0.072~g~L^{-1}, Tris~6.118~g~L^{-1}, and the pH is adjusted to 7.4. All the tests were carried out using an electrochemical workstation (Autolab, Metrohm, Switzerland) at room temperature.$

Table 1
Analyzed compositions of the studied ZnLiSr alloys and control group.

Nominal Composition (wt.%)	Analyzed Composition (wt.%)		
	Li	Sr	Zn
Zn0.8Li	0.79	N/A	Balance
Zn0.1Li0.1Sr	0.10	0.10	Balance
Zn0.1Li0.4Sr	0.10	0.42	Balance
Zn0.1Li0.8Sr	0.11	0.84	Balance
Zn0.4Li0.1Sr	0.38	0.09	Balance
Zn0.4Li0.4Sr	0.40	0.39	Balance
Zn0.4Li0.8Sr	0.79	0.83	Balance
Zn0.8Li0.1Sr	0.85	0.13	Balance
Zn0.8Li0.4Sr	0.85	0.42	Balance
Zn0.8Li0.8Sr	0.75	0.73	Balance

2.4.2. In vitro degradation tests

For the *in vitro* degradation tests, five parallel samples of each group were used. According to ASTM-G31-72, in this study the solution to area ratio was set at 20 mL cm $^{-2}$. The samples were immersed in SBF solutions at 37 $^{\circ}$ C for 90 days ($\approx\!12$ weeks). The solution was refreshed when there emerges precipitates in the solution, in case they may interfere with the degradation process. The pH values of the discarded solution were measured at the same time.

After the *in vitro* degradation tests, samples were rinsed with deionized water and dried in the air. Samples were analyzed with an X-ray diffractometer (XRD) to get the crystal structure of the degradation products. An SEM (S-4800, HITACHI, Japan) equipped with EDS was employed to get the microscopic images as well as chemical composition. FTIR method was applied to detect the characteristic chemical groups.

After the analyses, a solution containing 200 g/L CrO $_3$ was used to clean all the degradation products. Before and after the cleaning, the degradation morphology of the samples were imaged both at macroscale (using a 2.5 dimensional high precision imaging instrument) and under SEM. The weights of samples before and after the degradation process were measured. Based on the weight loss method, degradation rates could be calculated according to this equation: $C = \Delta m/(\rho \times A \times T)$, where C is the degradation rate (mm/year), Δm is the weight loss (g), ρ is the density of materials, A is the surface area of samples, and T is the duration of *in vitro* degradation tests.

2.5. In vitro biosafety tests

2.5.1. Cytocompatibility tests

Osteoblast precursor cell line (MC3T3-E1, ATCC CRL-2594TM) was selected to conduct the cytotoxicity tests and to evaluate the morphology of cytoskeleton. Prior to the tests, MC3T3-E1 cells were cultured in alpha-minimum essential medium (α -MEM) with the addition of 10% fetal bovine serum (FBS) and 1% penicillin-streptomycin. The extracts of alloys were prepared using cell culture medium, with a volume (of medium) to area (of sample surface) ratio at 1.25 mL cm $^{-2}$. The procedure lasted for 24 h, at 37 °C in a humidified atmosphere with 5% CO₂. Then the supernatant was centrifuged and kept at 4 °C before using.

MC3T3-E1 cells were seeded in 96-well plates at a density of 3×10^4 cells per well. Twenty-four hours later, in each well the culture medium was replaced with 100 μL of 100%, 50% and 10% sample extracts, respectively. Culture medium was chosen as negative control, and culture medium added with 10% dimethyl sulfoxide (DMSO, Invitrogen, USA) as positive control. After 1, 2, and 4 days' incubation, extracts (or culture medium in the control group) were refreshed with new culture medium, added with 10 μL of Cell Counting Kit-8 (CCK-8, Dojindo Molecular Technologies, Japan) per well. After 1 h's incubation in the cell incubator, a microplate reader (Bio-RAD680) was used to measure the optical density value (OD value) at the wavelength of 450 nm. For each group, at least five parallel measurements were taken.

2.5.2. Cell morphology evaluation

Cytoskeletal staining method using DAPI and FITC (Sigma-Aldrich, Germany) was applied to evaluate the cell morphology. Based on the results on CCK-8 tests, MC3T3-E1 cells cultured in 50% extracts for 24 h were studied. The stained cells were observed through a confocal laser scanning microscope (A1R–Si, Nikon, Japan).

2.6. In vitro osteogenic differentiation tests

2.6.1. ALP staining and quantitative analysis of ALP activity

MC3T3-E1 cells were seeded in 6-well plates at a density of 6×10^4 per well (3×10^4 mL⁻¹, 2 mL per well). After been incubated for 24 h in the cell incubator, and the cell fusion reached 80%, the cell culture medium was replaced with extracts of each group. Based on the results

of previously mentioned tests, Zn0.8Li0.1Sr extract was chosen as experimental group, $\alpha\text{-}MEM$ as well as extracts of Zn0.8Li and pure Zn were chosen as control groups. During the incubation, the extracts (or $\alpha\text{-}MEM$) were refreshed every 48 h. For each group, three wells were used. After 7 days and 14 days of being differentiation-induced, the extracts were discarded and the plates were rinsed gently with PBS for three times. The alkaline phosphatase (ALP) activity of MC3T3-E1 cells was then quantitatively evaluated using the ALP Quantitative Analysis Kit (Nanjing Jiancheng Bioengineering Institute, China). MC3T3-E1 cells cultured for 14 days following the same differentiation-inducing procedure were stained using the ALP Staining Kit (Shanghai Hongqiao Lexiang Institute of Biomedical Products, Shanghai, China) and then observed using an optical microscope (Olympus Co., Ltd., Tokyo, Japan).

2.6.2. Osteogenesis-related gene expression studies

Real-time PCR method was applied to illustrate the expression mechanism of osteogenesis-related genes in MC3T3-E1 cells. Cells were seeded and cultured in the same way as ALP tests. Based on the ALP activity results, extracts were diluted to 50% and 25% as to prepare the osteogenic induction solution. The entire induction process lasted for 10 days, with culture medium refreshed every 48 h. Subsequently, the mRNA expression levels of four marker genes: alkaline phosphatase (ALP), collagen type 1 (COL-1), osteocalcin (OCN) and Runt-related transcription factor 2 (Runx-2), were measured. Firstly, total RNA was extracted using RNeasy Mini Kit (Qiagen). Secondly, 1 mg RNA was reversed using a Reverse Transcription Kit (SuperScript™ III Reverse Transcriptase). The primer sequences are as shown in Supplementary Table 1. Thirdly, using the SYBR Premix Ex Taq II (2 \times) as PCR reagent, the real-time PCR was conducted on a ABI 7500 Fast machine (Applied Biosystems, Countaboeuf, France), under the conditions as-followed: 95 °C 30s; 95 °C 5s + 60 °C 40s, 40 cycles; dissolution curve, 95 °C $15s + 60\,^{\circ}\text{C}$ $60s + 95\,^{\circ}\text{C}$ 15s. Finally, the results were calculated through the $2^{-\Delta\Delta CT}$ method, where $\Delta\Delta Ct =$ (average Ct value of target gene in the test group - average Ct value of internal reference gene in the test group) – (average Ct value of target gene in the control group –average Ct value of control group).

2.6.3. Western blotting

Western blotting method was applied to measure the protein expression levels of ALP, COL-1, OCN and Runx-2. MC3T3-E1 cells were incubated following the same process as aforementioned, in extracts diluted to 50% for 10 days. Then cells were taken off the plate using a cell scraper, ice-bathed for 30min, and centrifuged at 12000 rpm for 10min. And the supernatant was collected as total protein. Specific primary antibodies against ALP, COL-1, OCN, Runx-2 and β -actin (as loading control) were diluted to 1:1000, and secondary antibodies were diluted to 1:7000, by TBST buffer respectively. The membranes were first incubated with primary antibodies at 4 $^{\circ}$ C overnight, and then with secondary antibodies at room temperature for 60min. The signals were detected using an Enhanced ChemiLuminescence Kit (ECL, Simuwubio, Shanghai, China).

2.7. In vivo osteoporotic-bone-fracture-treating studies (an OVX rat model)

2.7.1. Implants preparation

Based on the results of aforementioned *in vitro* studies, Zn0.8Li0.1Sr was selected as the candidate for further *in vivo* investigation. As to the selection of control group, pure Zn and Zn0.8Li alloy were first taken into consideration. However, their relatively poor mechanical strength and disappointing biocompatibility have already demonstrated them unideal for clinical usages, which means choosing them as control groups is meaningless for medical applications. Therefore, pure Ti, the gold standard material for orthopaedic repairs, was selected as control group. Both as-extruded Zn0.8Li0.1Sr and commercial pure Ti were

prepared into intramedullary nails in the shape of cylindrical rods ($\Phi=1.5\,$ mm, Height = 60 mm), with ends sharpened to facilitate the implantation procedure.

2.7.2. Procedures of animal model establishment

In order to explore the efficacy of Zn0.8Li0.1Sr alloy on treating osteoporotic bone fractures, an ovariectomized (OVX) rat model, which is considered the most popular animal model for osteoporotic bone fractures researches [39], was established. The entire procedure of animal model establishment is as shown in Fig.S1. First, 45 female Sprague-Dawley rats aged 12 weeks old, with an average weight of 283 \pm 10.5 g, underwent ovariectomy in accordance with previous protocol [40]. Ten rats randomly chosen from the same batch underwent no surgery, acting as a blank control group. Twelve weeks later, Micro-CT was employed to check the establishment of OVX rat model, by comparing the indices between the OVX group and the blank group. After confirming the OVX rat model has been successfully established, the implantation was carried out. Firstly, the rats were anesthetized by intraperitoneally injecting ketamine (10 mg/kg, Shanghai Ziyuan Pharmaceutical Co., Ltd, Shanghai, China) and 2% xylazine (5 mg/kg, Bayer, Leverkusen, North Rhine-Westphalia, Germany). Each rat's right hind limb was fixed (at a flexed position), shaved and depilated. After that, an incision about 2 cm long was introduced parallel to the femur. Then, the fascia was cut open, the muscles were bluntly separated along the intermuscular spatium, exposing the middle part of the femur. Using a medical saw, a fracture was created on the femoral shaft transversely. Then the femur was internally fixed using the aforementioned intramedullary nails made of Zn0.8Li0.1Sr or pure Ti, respectively. The fracture lines were placed carefully in good alignment. Among the rats, 20 were implanted with Zn0.8Li0.1Sr nails, and 20 were implanted with pure Ti nails as control group. Then the wound was carefully closed layer by layer, and each rat was given an X-ray scan to check the situation of surgery. Subsequently, each rat was injected with a 0.3 mg/kg dose of buprenorphine (Temgesic, Reckitt &Cloman, Hull, UK) as postoperative analgesia. The rats were then carefully reared until next procedures. All the operations and experiments related to animals had been ratified by the Animal Ethics Committee of Shanghai Rat & Mouse Biotech Co., Ltd.

2.7.3. X-ray observation and micro-computed tomography (Micro-CT)

To evaluate the conditions of implantation, 10 rats of each group were selected for analyses by 12 weeks and 24 weeks after the surgery, respectively. First, X-ray scanning was employed to evaluate the healing conditions of the fracture. Then the rats were sacrificed, whose right hind femurs were explanted and fixed with 4% paraformaldehyde. The femurs were then given a scan through Micro-CT (Scanco Micro-CT100, Switzerland). Subsequently, 3D reconstruction (Scanco $\mu100$ evaluation software) was performed to evaluate the healing conditions of the bone and the biodegradation of the implants. Region of interests (ROI) were defined as the circular bone tissue around the intramedullary nails within 0.5 mm. Quantitative analyses of the osteogenesis indices, including BMD (Bone Mineral Density), BV/TV (Percentage of Bone volume to Total volume), Tb.N (Trabecular Number), Tb.Th (Trabecular Thickness) and Tb.Sp (Trabecular Separation) were performed for the ROIs.

2.7.4. Histological evaluation

Following the Micro-CT scan, tissue slices were prepared, including 20 hard-tissue slices and 20 soft-tissue slices. For hard-tissue slicing (with implants), the specimens were rinsed with water, dehydrated with ethanol, washed with xylene, and finally embedded with methyl methacrylate (MMA). The cutting direction was parallel to the femurs' long axis. Then slices were performed with Van Gieson staining or Paragon staining, respectively. For soft-tissue slices (without implants), the specimens were decalcified and then embedded in paraffin. The slices were performed with Hematoxylin & eosin (HE) staining, Masson's

trichrome staining and Tartrate-resistant acid phosphatase (TRAP) staining. Simultaneously, 4 slices of each group were performed with immunohistochemical staining to evaluate the expression of ALP, COL-1, OCN and Runx-2. After that, a high-resolution microscope (Olympus Co., Ltd., Tokyo, Japan) was employed to observe and image the slices.

2.7.5. In vivo biosafety evaluation

For the experimental animals, crucial indicators including body temperature, body weight and wound healing conditions were recorded every day. After 24 weeks of the implantation, biological samples were collected from both the Ti group and the Zn0.8Li0.1Sr group, to evaluate the implants' in vivo biosafety. Firstly, arterial blood were collected from the rats using cardiac blood sampling method. Secondly, visceral organs, including the heart, liver, spleen, lung and kidney of the rats were collected, respectively. The concentrations of Zn^{2+} , Li^+ and Sr^{2+} in the blood serum and the visceral organs were measured with an ICP-Mass Spectrometry (ICP-MS, NexION 300Â, USA). Besides, slices of the organ tissues were prepared and performed with HE staining, and then their pathological changes were evaluated using an optical microscope. For each group, blood biochemistry tests were carried out. The 15 indices being examined include alanine aminotransferase (ALT), transglutaminase (AST), direct bilirubin (DBIL), total bilirubin (TBIL), albumin (ALB), alkaline phosphatase (ALP), gamma -glutamyl transpeptidase (Γ-GT), blood urea nitrogen (BUN), creatinine (CRE), uric acid (UA), total biliary acid (TBA), creatine kinase (CK), myocardial band of creatine kinase (CK-MB), L-lactate dehydrogenase (LDH-L) and lactate dehydrogenase-1 (LDH-1).

2.8. Statistical analysis

The data were analyzed through one-way analysis of variance (ANOVA) followed by Tukey post hoc tests. The results were presented as mean \pm standard deviation (n \geq 3, independent samples). A *p-value <0.05 was considered significant.

3. Results

3.1. Mechanical properties and microstructures

3.1.1. Mechanical properties

Fig. 1(a) shows the stress-strain curves of pure Zn, Zn0.8Li and Zn0.8Li0.1Sr. Zn0.8Li0.1Sr exhibits a higher ultimate tensile strength (UTS), and a lower Young's modulus than Zn0.8Li. Fig.1(b) and Fig.S2 (b) show the results of strength and ductility obtained from tensile tests. Among the alloys being tested, the highest UTS belongs to Zn0.8Li0.1Sr (524.33 \pm 18.01 MPa), which is almost 7 times that of pure Zn (73.06 \pm 4.18 MPa), and 12.4% higher than that of Zn0.8Li (466.57 \pm 12.82 MPa). The results suggests that the addition of Li and Sr can significantly improve the strength of Zn alloys. The ductility (δ) of Zn0.8Li0.1Sr is $24.98 \pm 9.68\%$, which represents a large improvement from that of pure Zn (6.54%). Fig.1(c) and Fig.S2(c) show the results of Vickers hardness tests. It can be seen that, the more Li added, the higher Vickers hardness the alloy has. The Vickers hardness of tertiary Zn0.8Li0.1Sr (132.60 \pm 9.08 HV) is significantly lower than that of Zn0.8Li (173.90 \pm 8.60 HV), which means the addition of Sr have brought a softening effect to the binary Zn0.8Li alloy.

3.1.2. Microstructures

Fig.1(d) and Fig.S2(d) show the X-ray diffraction (XRD) results. The main phases of ZnLiSr alloys are α -Zn, LiZn₄, and SrZn₁₃. Fig.1(e) and Fig.S2(e) show the microstructures of Zn alloys obtained from metallographic analyses. The as-cast alloys have large grains or dendritic structures. It can be clearly observed that the as-extruded alloys have finer grains and river-like patterns. In alloys with a higher Sr amount (0.4 wt% or 0.8 wt%), there still remained large grains of second phases (about 50–100 μ m) after the extrusion. While in the as-extruded

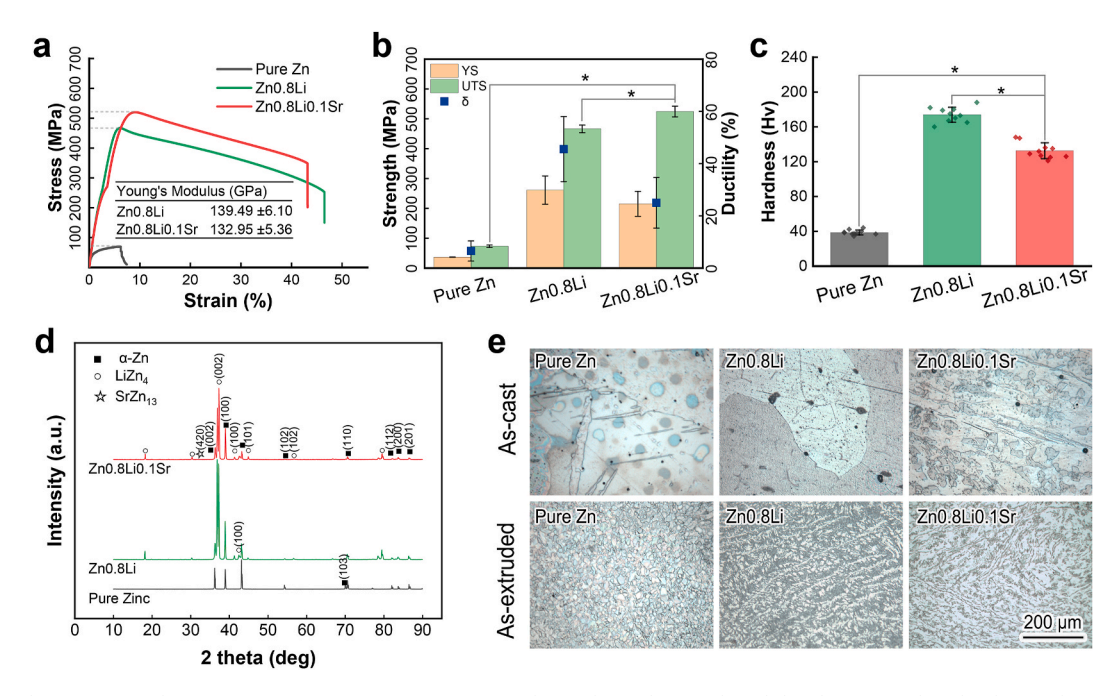


Fig. 1. Mechanical properties and microstructures. (a) Stress-strain curves; (b) Mechanical strength and ductility; (c) Vickers hardness; (d) X-ray diffraction; (e) Metallographic analyses. The data were expressed as mean \pm standard deviation (SD). n = 4 in panel (b); n = 10 in panel (c). *: p < 0.05.

Zn0.8Li0.1Sr, there exhibited only uniform river-like patterns, which suggests that Zn0.8Li0.1Sr possess a more homogeneous microstructure.

3.2. In vitro degradation behavior analyses

3.2.1. Electrochemical tests

Fig. 2(a) shows the results of Tafel polarization tests. Zn0.8Li0.1Sr has a higher open circuit potential (OCP) than the control groups, which means that Zn0.8Li0.1Sr is more difficult to be corroded under the same potential. Fig. 2(b) shows the results of impedance spectroscopy tests. Zn0.8Li0.1Sr exhibits a larger impedance spectroscopy loop than the control groups, which means that Zn0.8Li0.1Sr has a stronger resistance to degradation in the SBF environment.

3.2.2. In vitro degradation tests

Fig. 2(c) shows the *in vitro* degradation rates calculated using weight loss method. Zn0.8Li0.1Sr has a lower degradation rate (10.13 \pm 1.52 μm year $^{-1}$) than that of pure Zn (12.66 \pm 1.00 μm year $^{-1}$) and Zn0.8Li (16.38 \pm 1.75 μm year $^{-1}$). After the *in vitro* degradation tests, the morphology of samples were studied both before and after the cleaning of degradation products. Fig. 2(d) shows the degradation morphology after the *in vitro* degradation tests in a macro scale. It can be seen that there are more corrosion pits on the surface of pure Zn and Zn0.8Li, while Zn0.8Li0.1Sr exhibits a much more uniform degradation morphology. Fig. 2(e) shows the degradation morphology under SEM. The Zn0.8Li alloy has an obviously rougher degradation morphology and larger corrosion pits, while the surface of Zn0.8Li0.1Sr after *in vitro* degradation test is relatively uniform. All these results show Zn0.8Li0.1Sr manifests a more mild and uniform degradation behavior.

3.2.3. Chemical analyses of the in vitro degradation products

Fig. 2(f) shows the XRD results of samples after *in vitro* degradation tests. The main compositions of degradation products are ZnO and CaCO₃. Fig. 2(g) shows the FTIR results of degradation products. The main chemical groups of degradation products are H–O, $\rm CO_3^{2-}$, $\rm PO_4^{3-}$, and Zn–O. The FTIR results further confirmed the XRD results that ZnO and CaCO₃ are the main degradation products of Zn alloys in SBF.

3.3. Cytocompatibility

Fig. 3(a)-(c) shows the results of CCK-8 tests. The 100% extracts brought about inhibition of the MC3T3-E1 cells' activity. While in the extracts diluted to 50% and 10%, cells manifested good growing states compared to the negative control group (cells cultured in α -MEM). Fig. 3 (d) shows the cell morphology obtained from cytoskeletal staining. Compared with cells cultured in α -MEM, the cells cultured in three kinds of 50% alloy extracts showed similar shapes and spreading states, which suggests that the as-tested 50% extracts are biologically safe for MC3T3-E1 cells. Compared to the control groups, the cells number of the Zn0.8Li0.1Sr group is higher. Besides, the cells manifested a healthier spreading state, with larger spreading area of cells in the Zn0.8Li0.1Sr group. This result means that Zn0.8Li0.1Sr alloy is more favorable for the growth of MC3T3-E1 cells than pure Zn or Zn0.8Li alloy.

3.4. In vitro osteogenic differentiation

3.4.1. Quantitative analyses of ALP activity and ALP staining

Fig. 4(a)(b) display the results of ALP staining results obtained from MC3T3-E1 cells cultured in 50% and 25% extracts, respectively. All groups showed obviously positive staining results, suggesting that there were massive expression of ALP in these groups. Fig. 4(d)(e) display the ALP activity of MC3T3-E1 cells cultured in 50% and 25% extracts, respectively. These two groups showed a significant increase of ALP activity from 7th day to 14th day. For the 14th day's results, the ALP activity of Zn0.8Li0.1Sr groups are significantly higher than those of Zn0.8Li groups. The ALP results show that the Zn0.8Li0.1Sr induced stronger osteoblastic differentiation than the Zn0.8Li group for the MC3T3-E1 cells.

3.4.2. Western blotting and osteogenesis-related gene expression

Fig. 4(c) displays the results of western blotting. The results reveal that the expression levels of ALP, COL-1 of Zn0.8Li0.1Sr are higher than those of control groups. Moreover, there exhibit distinct up-regulations of OCN and Runx-2 in all three alloys than those of α -MEM, suggesting that the release of ions from the alloys could activate the expression of these typical proteins. Fig. 4(f)–(i) display the expression levels of four critical genes relative to osteogenesis: ALP, COL-1, OCN, and Runx-2.

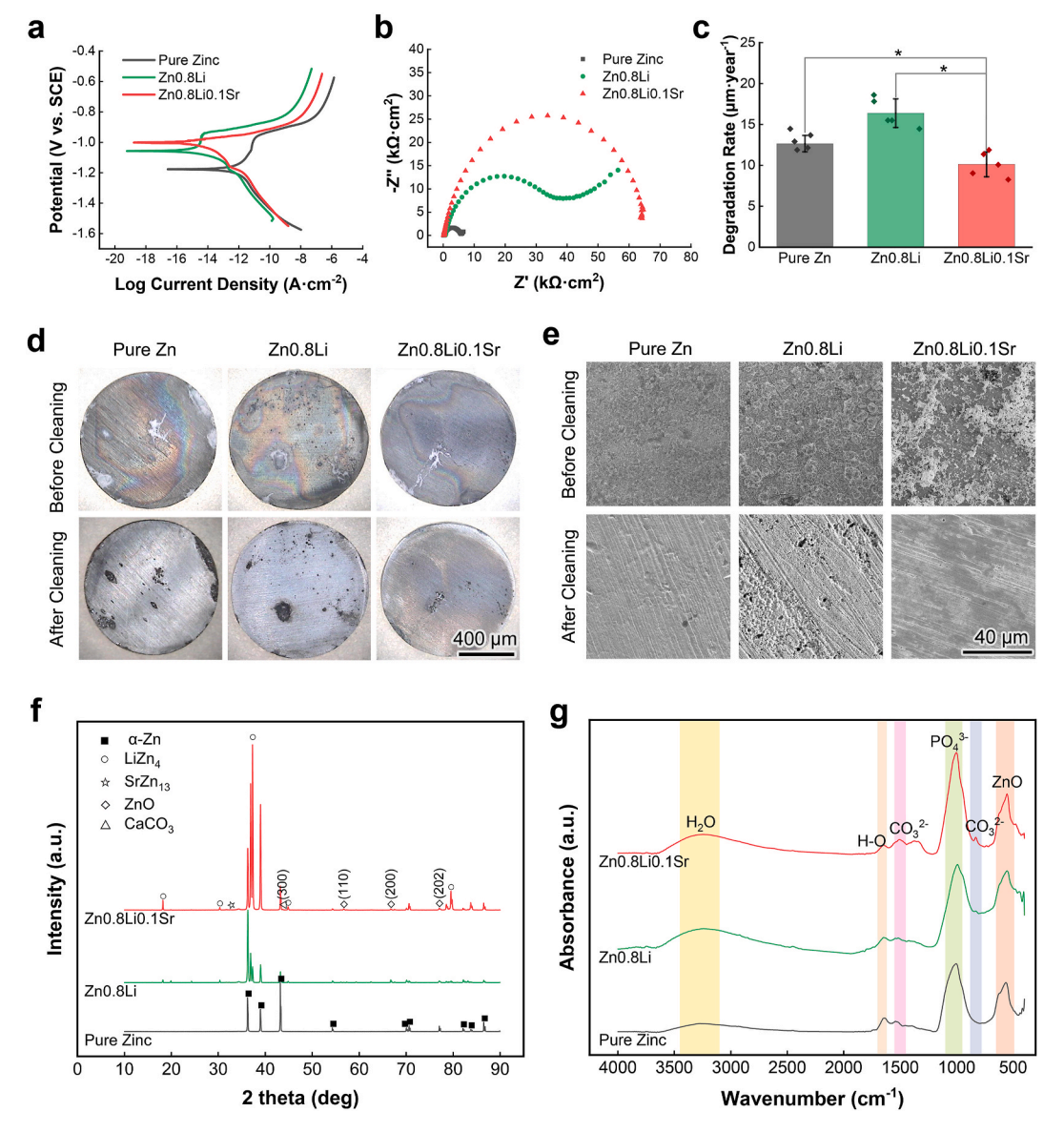


Fig. 2. Electrochemistry and *in vitro* degradation tests. (a) Tafel polarization curves; (b) Impedance spectroscopy; (c) Degradation rates calculated through weight loss method; (d) Degradation morphology in macro-scale; (e) Degradation morphology under SEM; (f) XRD results of degradation products; (g) FTIR results of degradation products. The data (n = 5) were expressed as mean \pm standard deviation (SD). *: p < 0.05.

The expression levels of all these four genes in the Zn0.8Li0.1Sr group are significantly higher than those in the other three groups, revealing that Zn0.8Li0.1Sr alloy has up-regulated these osteogenesis-related genes more than the control groups.

3.5. X-ray imaging and micro-CT

For the conciseness of this paper, in the later text, code names were used to represent groups as followed: T-12 for rats implanted with pure Ti at 12 weeks, T-24 for rats implanted with pure Ti at 24 weeks; Z-12 for rats implanted with Zn0.8Li0.1Sr at 12 weeks, Z-24 for rats implanted with Zn0.8Li0.1Sr at 24 weeks.

3.5.1. The healing conditions of OVX rats' bone fractures

As the X-ray scanning results (Fig. 5(a)) and the 3D reconstruction results (Fig. 5(c)) show, after 12 weeks of the implantation, there still existed an obvious fracture line in the T-12 group, while the fracture of Z-12 group was almost recovered, suggesting a better healing status in the Z-12 than in the T-12 group. Fig. 5(b) shows the explanted femur

bones. In both the T-24 group and the Z-24 group, the fracture lines have healed, which indicates that Zn0.8Li0.1Sr has successfully healed the bone fracture as well as the pure Ti. Besides, in the T-24 group, there appeared red-colored tissue among the fracture line position, suggesting that the bone had not accomplished the whole healing process. While in the Z-24 group, the whole bone, including the fracture line position, exhibits a healthy appearance in the same white color.

3.5.2. Analyses of osteogenesis indices obtained from Micro-CT

Fig. 5(d) shows the quantitative analysis of 5 osteogenesis indices obtained from Micro-CT. In each diagram, the first group of bars was the result of OVX rat modeling verification. There exhibited significant differences in key indices, including BMD, BV/TV and Tb.Sp, between the blank group (black bars) and OVX group (blue bars), proving that the OVX rat model was successfully established. After 12 weeks of the implantation, three indices, including BMD, BV/TV and Tb.Th of Z-12 group are significantly higher than those of T-12 group, which means that Zn0.8Li0.1Sr alloy caused stronger osteogenesis inducement than pure Ti. Another index Tb.Sp of Z-12 group is lower than that of the T-12

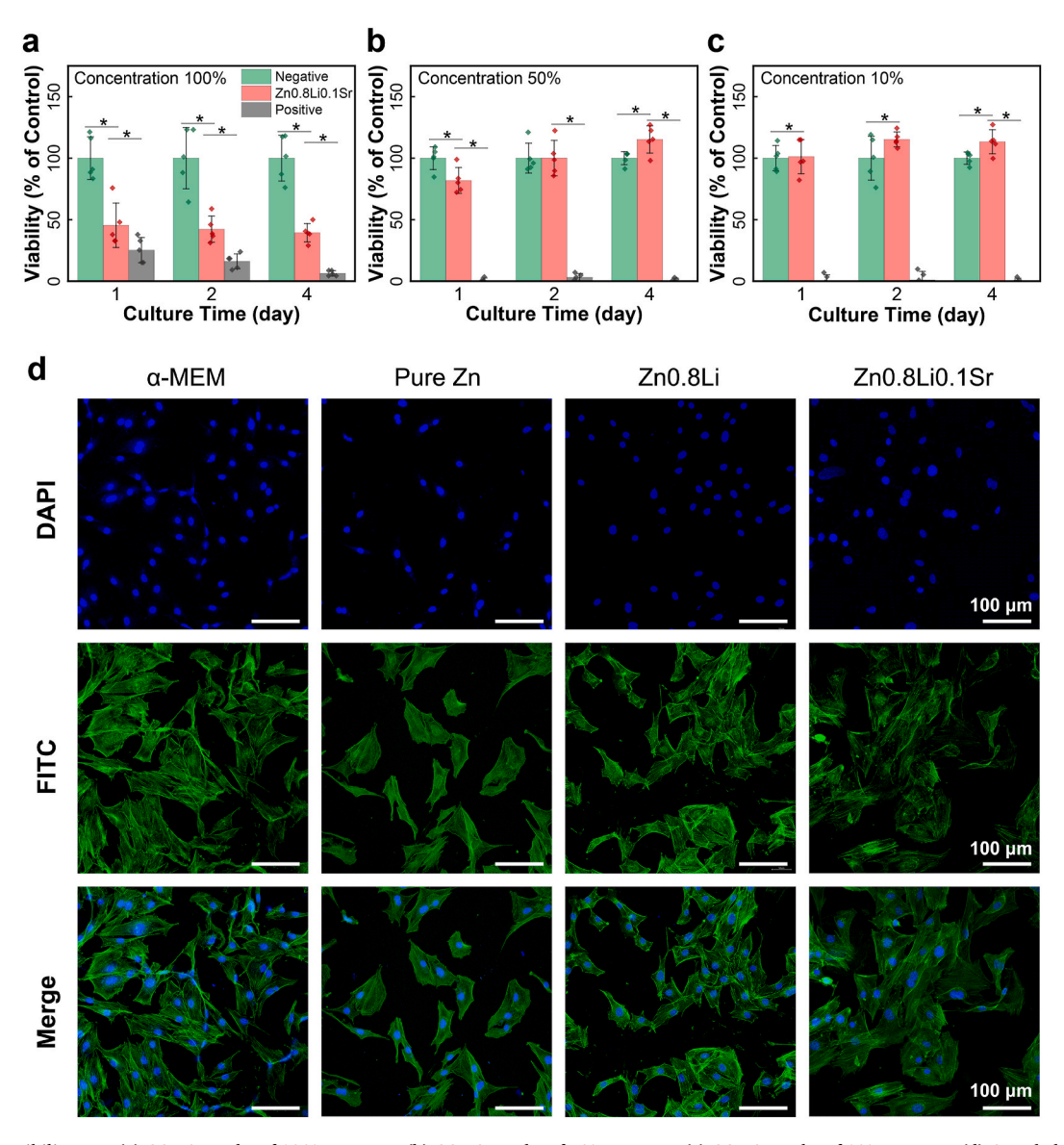


Fig. 3. Cytocompatibility test. (a) CCK-8 results of 100% extracts; (b) CCK-8 results of 50% extracts; (c) CCK-8 results of 10% extracts; (d) Cytoskeletal staining. The data (n = 5) were expressed as mean \pm standard deviation (SD). *: p < 0.05.

group, which means there was lower separation of trabeculae in the Z-12 group. All these data confirmed that Zn0.8Li0.1Sr induced osteogenesis superior than pure Ti in the OVX rats. After 24 weeks of the implantation, the osteogenesis indices were all improved compared to the 12 weeks' results, showing that in all groups the bone underwent good healing process. The Tb.N, BV/TV and BMD of the Z-24 group are higher than those of the T-24 group, as well as the Tb.Sp of the Z-24 group is lower than that of the T-24 group. The 24 weeks' results further confirmed that Zn0.8Li0.1Sr alloy caused osteogenesis inducement better than pure Ti.

3.5.3. In vivo biodegradation of the intramedullary nails

Fig. 5(c) also shows the reconstruction results of ROIs and the implants. In the fourth row of Fig. 5(c), the metallic parts in the samples, including the intramedullary nails as well as their biodegradation products, were reconstructed in yellow color. It can be clearly seen that pure Ti intramedullary nails had not been biodegraded neither in the T-12 group nor in the T-24 group. For the Zn0.8Li0.1Sr nails, there were a small amount of biodegradation products around the nails at 12 weeks, and considerable biodegradation products were amassed around the nails at 24 weeks. This revealed the Zn0.8Li0.1Sr intramedullary nails

has undergone more significant biodegradation process than the pure Ti nails.

3.6. Histological evaluation

3.6.1. Histological evaluation of tissue hard-tissue slices

Fig. 6(a) shows the Van Gieson staining results. For the pure Ti groups, both results of T-12 group and T-24 group showed that the pure Ti nails remained intact during the entire implantation period, and there existed no obvious interaction between the intramedullary nail and the surrounding bone tissue. For the Zn0.8Li0.1Sr groups, the results of Z-12 group indicated that next to the biodegradation products there emerged a new layer of collagen (stained into purple), which reveals that the osteoblasts were stimulated to synthesize new collagen concomitant with the biodegradation process of Zn0.8Li0.1Sr alloy. In the Z-24 group, the collagen tissue became thinner, while the osteoid and new bone (stained into red) tissue became obviously thicker. These results reveal that the Zn0.8Li0.1Sr alloy and its biodegradation products outperformed pure Ti as to induce the synthesis of collagen which would later grow into new bone tissue.

Fig. 6(b) shows the Paragon staining results. The Paragon staining

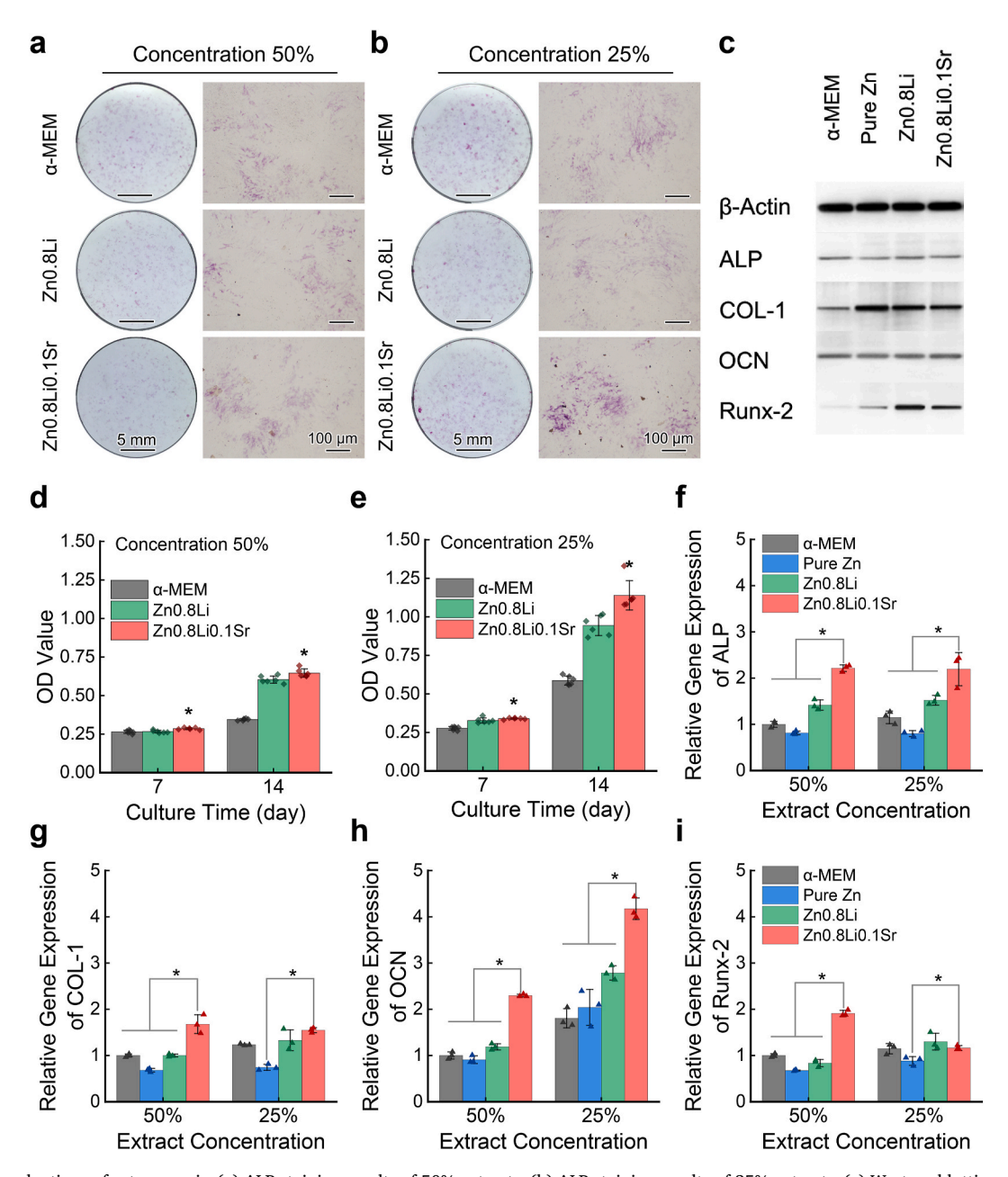


Fig. 4. In vitro evaluations of osteogenesis. (a) ALP staining results of 50% extracts; (b) ALP staining results of 25% extracts; (c) Western blotting; (d) Quantitative analysis of ALP expression in 50% extracts; (e) Quantitative analysis of ALP expression in 25% extracts; (f)–(i) The relative gene expression levels of ALP, COL-1, OCN and Runx-2. The data were expressed as mean \pm standard deviation (SD). n = 6 in panels (d) and (e); n = 3 in panels (f)–(i). *: p < 0.05.

method could distinguish between nuclei and cytoplasm, as well as indicate the new bone tissue. For 12 weeks' results, the Z-12 group exhibited a thick layer of osteoblasts (stained into violet) close to the intramedullary nail, while in the T-12 group there existed no obvious osteoblasts. For 24 weeks' results, the new bone tissue (honeycomb-like tissue stained into pink) of the Z-24 group has apparently thickened, and clusters of osteoblasts (the violet particles) were distributed inside the new bone tissue. However, in the T-24 group there showed no obvious proliferation of osteoblasts. These results reveal that the Zn0.8Li0.1Sr alloy has superior efficacy than pure Ti as to increase the proliferation of osteoblasts.

3.6.2. Elements distribution of hard-tissue slices

The EDS mapping results of hard-tissue slices, which display the distribution of element C, O, P, Ca, Sr, as well as the main elements for two groups: Ti element for the pure Ti group, and Zn element for the

Zn0.8Li0.1Sr group, are as shown in Fig. 6(e)(f). To make it clear, element Li was not detected due to the limitation of state-of-the-art EDS technique, which could not give precise analyses of light elements such as H, Li and B. From the results it can be apparently seen that, for the pure Ti groups, both the intramedullary nail of the T-12 group and the T-24 group remained as intact as it had been just implanted. The distribution of elements indicates a clear and straight boundary between the intramedullary nail and the ambient bio-tissue, suggesting there existed no interference between them.

For the Zn0.8Li0.1Sr groups, in the Z-12 group, the boundary between the intramedullary nail and ambient bio-tissue was still relatively straight, suggesting that the intramedullary nail still remained intact and was providing mechanical supports at full length then. However, in the Z-24 group, the boundary became broken. Amid the boundary, there manifested considerable biodegradation products. Combined with the aforementioned results, a conclusion could be drawn as: the

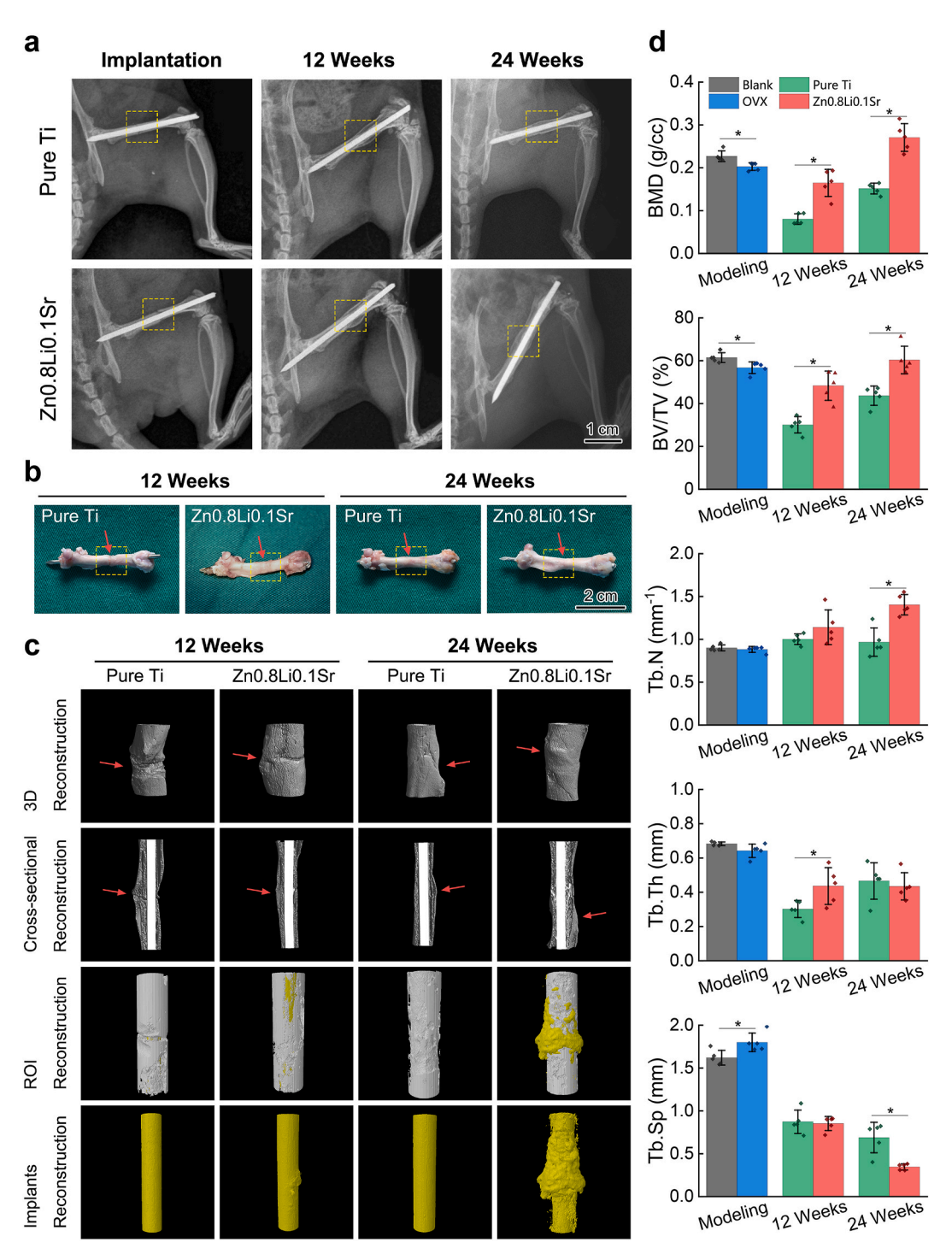


Fig. 5. Animal test results. (a) X-ray scanning images; (b) Explanted femur bones; (c) Micro-CT 3D reconstructions; (d) Quantitative analyses of osteogenesis indices calculated from Micro-CT. The data (n = 5) were expressed as mean \pm standard deviation (SD). *: p < 0.05.

Zn0.8Li0.1Sr intramedullary nail remained relatively intact when the bone need more mechanical support (at 12 weeks), and started to be biodegraded at the juncture when the bone almost healed and needed enough load to regain its strength (at 24 weeks). The EDS mapping results of element P and Ca indicate the positions where new bone tissue formed. In Zn0.8Li0.1Sr groups, the EDS signal intensity of P and Ca are higher than those of pure Ti groups, indicating that there had formed a greater amount of new bone in the Zn0.8Li0.1Sr group than in the pure Ti group.

Line scan EDS was performed for the same region of Z-24 group. Fig. 6(g) shows the line scan direction for the slice, in which the ROI was

divided into four areas according to the EDS mapping results and Paragon staining results. Fig. 6(h) shows the EDS line scan results. In the Zn0.8Li0.1Sr area, the signal intensity of Zn is significantly high, while the O, P and Ca exhibited very low intensities. In the biodegradation products area, the signal intensity of Zn is still significantly high, while there appeared an increase of O intensity. In the osteoid area, the signal intensity of Zn and O rapidly decreased and the intensities of P and Ca exhibited a tendency to increase. In the new bone area, the signal intensities of Ca and P obviously increased, while the element Zn showed a low signal intensity. The same line scan analyses were performed for T-12, Z-12 and T-24 groups, the results are as displayed in Fig.S7. As Fig.S7

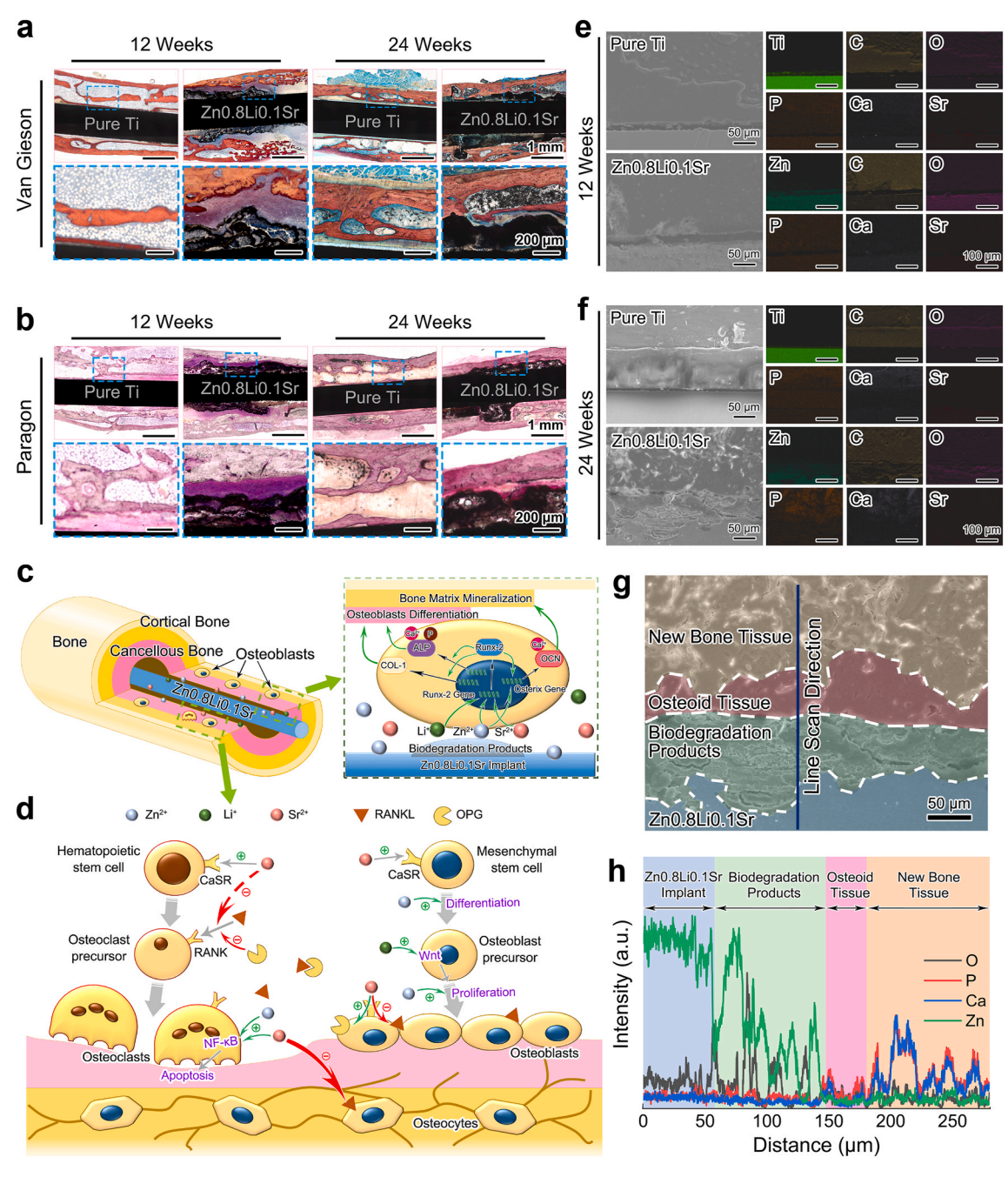


Fig. 6. Analyses of hard-tissue slices and illustrations of osteogenesis-inducing mechanism. (a) Van Gieson staining; (b) Paragon staining. (c) The gene-stimulation mechanism by Zn^{2+} , Li^+ and Sr^{2+} in an osteoblast; (d) The influences of Zn^{2+} , Li^+ and Sr^{2+} on bone remodeling. (e) EDS mapping of 12 weeks' results; (f) EDS mapping of 24 weeks' results; (g) A colored rendering indicating the EDS line scan within the SEM image of 24 weeks' results; (h) EDS line scan results.

(a)(b)(e)(f) show, the signal intensities of O, P and Ca are consistently low in T-12 and T-24 groups. No clear formation of layers could be observed.

3.6.3. Histological evaluation of soft-tissue slices

Fig. 7(a) shows the HE staining results. For 12 weeks' results, in the T-12 group there still remained a clear unhealed fracture line (indicated as ROI labeled with a blue box). In the Z-12 group, there appeared newly synthesized collagen tissue (stained into pink) around the intramedullary nail, and a greater number of osteoblasts emerged in this layer. For 24 weeks' results, firstly both the T-24 group and Z-24 group showed no obvious fracture line, indicating a good healing state in both groups. The thickness of femur bone in the T-24 group exhibited no significant differences from that of the T-12 group, while there was an

apparently enlargement of callus in Z-24 group. As the ROIs show, the collagen once close to the intramedullary nail in the Z-12 group has grown into new trabecular bone (the honeycomb-like tissue stained into purple).

Fig. 7(b) shows the Masson staining results. For the 12 weeks' results, in T-12 group there were little newly formed collagen (stained into blue), except in the fracture line region. However, the outer layer in the Z-12 group comprised plenty of collagen, and thus thickening the femur bone. For the 24 weeks' results, in the T-24 group there formed a thin layer of collagen. While in the Z-24 group, the callus comprised both collagen and a high number of osteocytes (whose cytoplasm were stained into red).

Fig. 7(c) shows the TRAP staining results. In the T-12 group, there were plenty of osteoclasts (stained into claret) at the fracture line. While

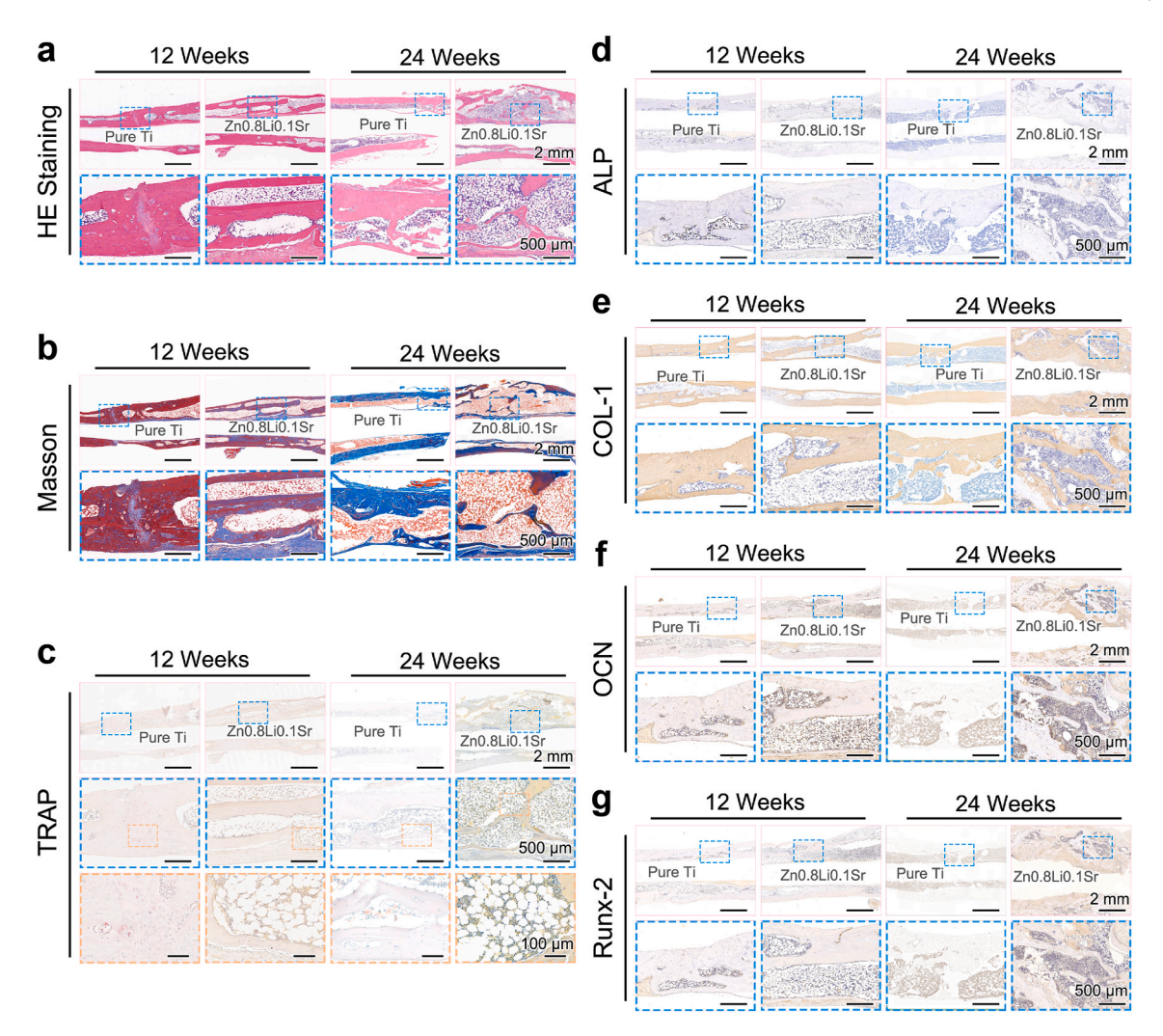


Fig. 7. Analyses of soft-tissue slices and immunohistochemical staining. (a)–(c) Soft-tissue slices of HE staining, Masson staining and TRAP staining; (d)–(g) Immunohistochemical staining of ALP, COL-1, OCN and Runx-2.

in the Z-12 group, there were no obvious osteoclasts. In the T-24 group, there still existed osteoclasts in the trabeculae. However, in the Z-24 group there exhibited no evident existence of osteoclasts. These results reveal that, in the pure Ti groups, there stimulation of osteoclasts were considerable. While in the Zn0.8Li0.1Sr groups, the activity of osteoclasts were inhibited.

3.6.4. Immunohistochemical analyses

The immunohistochemical analyses of four critical indices, including ALP, COL-1, OCN and Runx-2, are as displayed in Fig. 7(d)–(g). The semi-quantitative analyses of immunohistochemical slides, including positive ratios and H-scores, are as displayed in Fig.S8.

ALP is a vital marker to identify the activity of osteoblasts. COL-1 is an essential structural component of the new bone tissue. ALP and COL-1 were expressed mainly during the differentiation of osteoblasts [41]. As shown in Fig. 7(d) and (e), for 12 weeks' results, there showed higher expression of ALP and COL-1 in the Z-12 group than in the T-12 group. For 24 weeks' results, the expression levels of ALP and COL-1 in the newly grown trabecular bones were also higher in the Z-24 group than in the T-24 group. These results reveal that Zn0.8Li0.1Sr alloy promoted osteoblast differentiation further than pure Ti.

OCN is a critical protein which was mainly expressed during the bone mineralization [41]. As Fig. 7(f) shows, the expression level of OCN in the Zn0.8Li0.1Sr group is higher than that in the pure Ti group both at 12 weeks and 24 weeks, indicating a better mineralization status of the

bone matrix in Zn0.8Li0.1Sr groups than in pure Ti groups.

Runx-2 plays a key role in the regulation of osteoblast gene expressions, and Runx-2 can up-regulate the expression of ALP, COL-1 and OCN [42]. As Fig. 7(g) shows, the expression of Runx-2 were much higher in Zn0.8Li0.1Sr groups than in the pure Ti groups both at 12 weeks and at 24 weeks. A conclusion could be drawn from all these immunohistochemical results as: For the aspect of osteogenesis-inducing, Zn0.8Li0.1Sr alloy outperformed pure Ti for both the differentiation of osteoblasts and the mineralization of bone matrix, thus generating a better healing condition and a faster growth rate of bone in animals with osteoporotic bone fractures.

3.6.5. In vivo biosafety

For the *in vivo* biosafety of biomaterials, systemic evaluations are requisite [43]. Fig. 8(a) shows the histological slices of collected organs from the sacrificed rats, including the heart, liver, spleen, lung and kidney. The HE staining results reveal that the morphology of these organs exhibited no obvious differences between the pure Ti group and the Zn0.8Li0.1Sr group. Fig. 8(b) shows the ICP results measuring the ion concentrations in the blood and the five aforementioned organs. For Zn²⁺, Li⁺ and Sr²⁺, there exhibited no significant differences in the concentration levels between the pure Ti group and Zn0.8Li0.1Sr group. The results of blood biochemistry tests are as shown in Fig. 8(c). For all the items being tested, there exhibited no significant differences between the pure Ti groups and the Zn0.8Li0.1Sr groups, both at 12 weeks

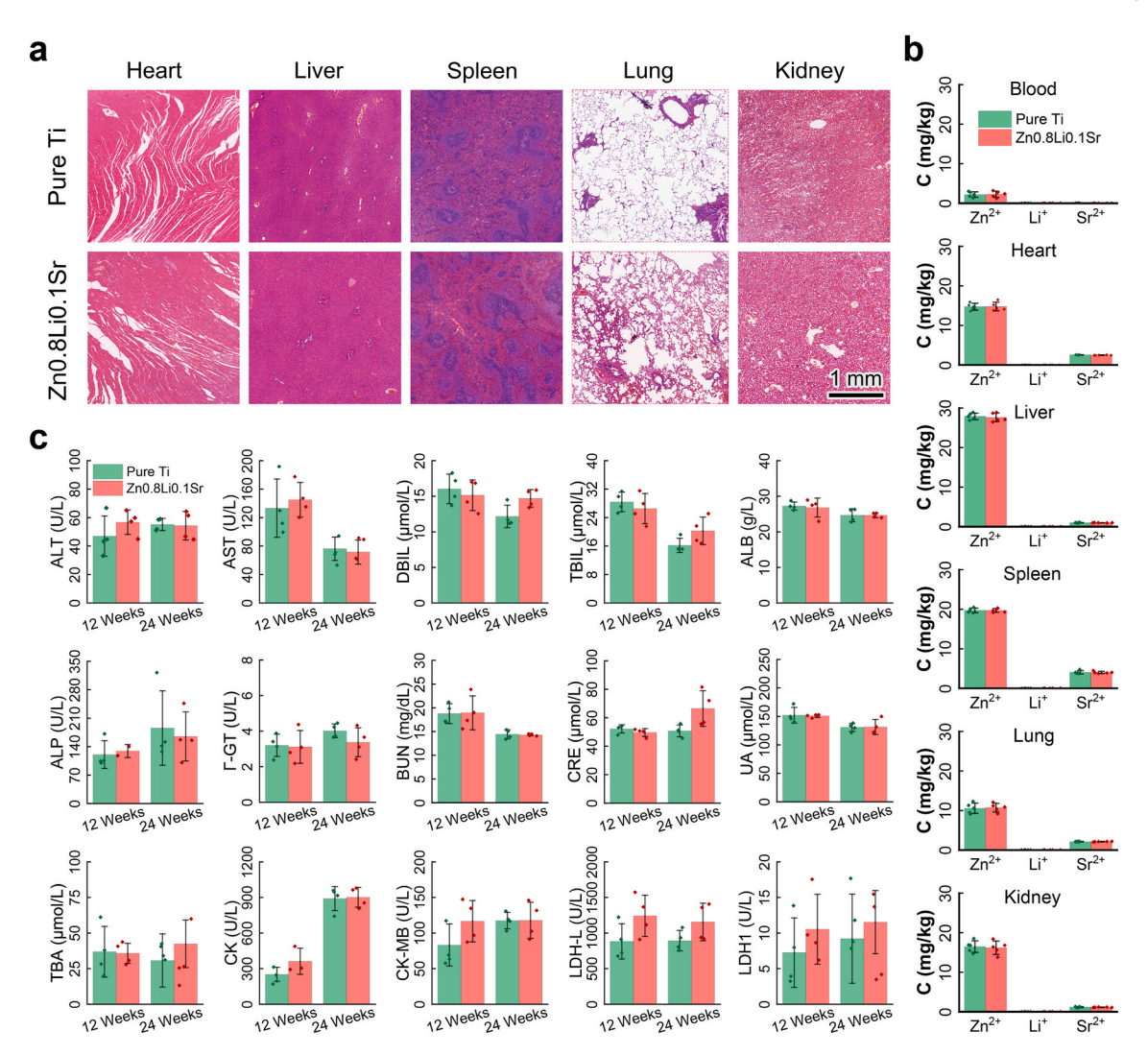


Fig. 8. In vivo biosafety. (a) Histological evaluations of organs; (b) ICP results of Zn^{2+} , Li^+ and Sr^{2+} in blood and five organs (C: concentration); (c) Blood biochemistry test results. The data were expressed as mean \pm standard deviation (SD). n = 5 in panel (b); n = 4 in panel (c). *: p < 0.05.

and at 24 weeks. All these histological and biochemical results indicate that, as to the aspect of *in vivo* biosafety, Zn0.8Li0.1Sr alloy and pure Ti were at a similar level.

4. Discussion

4.1. Mechanical properties, stress-shielding and biodegradation

Biodegradable metal has been a hot topic of biomaterials researches since the last decade. And there have already emerged medical devices made of biodegradable metals, such as the bone screws made of MgCaZn [44] and MgZnYEr [45] ratified by the Korea Food and Drug Administration (KFDA) and Conformité Européene (CE), respectively. Nonetheless, the unsatisfactory mechanical properties of previously studied biodegradable metals still failed the requirements of load-bearing applications, thus limiting their usages to a very small domain. To improve the mechanical properties of biodegradable metals, both the strength and the ductility should be enhanced. However, there exists an conflict between these two properties, usually causing a dilemma where enhancing the strength would contemporarily reduce the ductility [46,

A widely accepted index that measures the comprehensive mechanical properties of materials is the strength-ductility balance (GPa%) [48,49], which is the product of multiplying the strength (MPa) and the

ductility (%). The mechanical properties of previously reported Mg alloys [5,34,50-56], Zn alloys [13,19,21,23,26,28,55,57-68], Fe alloys [5,13,65,69-71] and the ZnLiSr alloys in this paper are displayed in Fig. 9. The strength-ductility balances of most previously reported biodegradable metals are below 10 GPa%, among which the Mg alloys (the vellow area) have lower strength-ductility balances around only 6 GPa%. Compared to Mg alloys, Zn alloys have shown superior mechanical properties, among which the strength of ZnLi alloys (the blue area) has been significantly increased. Although ZnLi alloys exhibited higher strength, their ductility still demands improving. In contrast to these biodegradable metals, ZnLiSr alloys possess both improved strength and ductility, among which the strength-ductility balance of five alloys (Zn0.8Li0.1Sr, Zn0.4Li0.1Sr, Zn0.4Li0.4Sr, Zn0.1Li0.8Li and Zn0.1Li0.1Sr) have surpassed 10 GPa%. The addition of Sr have significantly improved the ductility as well as the strength-ductility balance of ZnLi alloys. The superb comprehensive mechanical properties of ZnLiSr alloys make them suitable candidates to be used in load-bearing positions.

For the recovery of bone fractures, a medical implant with high mechanical strength may play a role of two-edged sword. On the first stage when the bone needs enough external support to repair its broken structures, a higher strength of the medical implants could promise a more smooth recovery process. However, after the bone has almost healed, the task has been altered from repairing the structure to

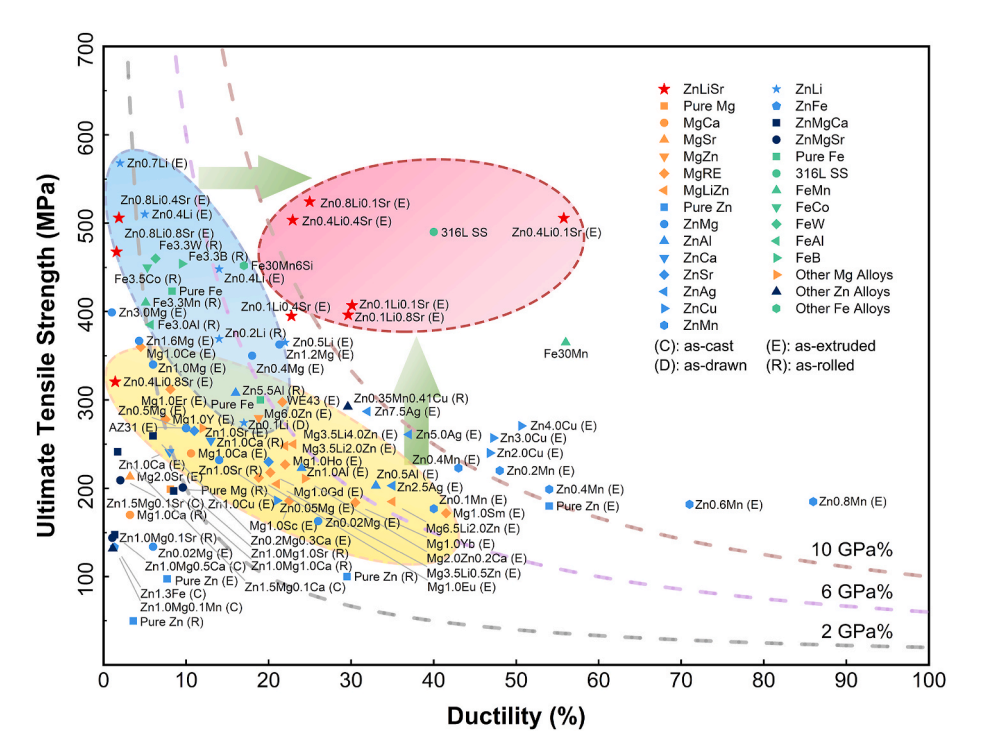


Fig. 9. Comprehensive mechanical properties of biodegradable metals, including Mg alloys [5,34,50–56], Zn alloys [13,19,21,23,26,28,55,57–68], Fe alloys [5,13,65,69–71] and the ZnLiSr alloys in this paper.

regaining the strength. At that time, an implant of high-strength would do little favor. On the contrary, it might cause the well-known trouble as stress-shielding. Hence, an ideal medical implant should adapt its role to the different needs of each fracture recovery stage. During the first stage, the implant should remain intact and provide enough support to heal the bone fractures. During the second stage, the implant should be well biodegraded with its strength gradually reduced, letting the bone undertake necessary stress to regain its strength [8]. As Fig. 1(b) shows, Zn0.8Li0.1Sr possess an ultimate tensile strength of 524.33 \pm 18.01 MPa, which is comparable with the strength of commercial pure Ti (≈500 MPa) [72]. The high mechanical strength of Zn0.8Li0.1Sr suggests that it can serve well in load-bearing positions, providing enough supports for the fractured bone during the first stage. The in vivo implantation results proved that, after 12 weeks of the implantation, the Zn0.8Li0.1Sr provided good mechanical supports for the OVX rats' femur bones.

The Young's modulus of the implant, which has a great influence over the activities of osteocytes [73], is another mechanical property to be concerned. A lower modulus of the metal implant is beneficial for the bone to avoid stress-shielding problems [72]. As Fig. 1(a) shows, the Young's modulus of Zn0.8Li0.1Sr was lower than that of Zn0.8Li. The Vickers hardness (Fig. 1(c)) of Zn0.8Li0.1Sr is also lower than that of Zn0.8Li. These results revealed that the addition of Sr has brought a softening effect to the ZnLi alloys.

An implant with mild and uniform degradation behaviors means that the changes in mechanical properties would be steady and the service *in vivo* would be more reliable. As Fig. 2(d)(e) and Fig.S3 shows, the corrosion pits of Zn0.8Li0.1Sr are both lower in number and smaller in dimension than the pure Zn and Zn0.8Li. The degradation morphology of Zn0.8Li0.1Sr is relatively smooth and uniform. Since it is the corrosion pits that often serve as positions for stress concentration [74], less corrosion pits implies that Zn0.8Li0.1Sr possess a lower likelihood of suffering from abrupt failure. Therefore, Zn0.8Li0.1Sr would be more reliable to serve as *in vivo* implants than the control groups.

After the first stage of bone-fracture healing, the implants need to reduce its mechanical strength via gradual biodegradation to achieve closer mechanical properties with the bone [75,76]. On this stage,

Zn0.8Li0.1Sr alloy manifested significant advantages over pure Ti. As Fig. 5 shows, the femur bone of Z-24 group grew thicker, and the enlargement of callus in the Z-24 group indicates that Zn0.8Li0.1Sr alloy together with its biodegradation products have induced osteogenesis in the femur bone of OVX rats, which is seldom seen in animals with osteoporotic bone fractures. At the meantime, the biodegradation process decreased the Zn0.8Li0.1Sr intramedullary nails' mechanical strength, transferring more necessary loads to the bone. The combination of these two functions resulted in a higher bone thickness and a higher number of osteoblasts in the Z-24 group.

4.2. The osteoporotic-bone-fracture-treating mechanism of Zn0.8Li0.1Sr

Previous studies have elucidated the mechanism of $\rm Zn^{2+}$, $\rm Li^+$ and $\rm Sr^{2+}$ regulating osteogenesis-related genes, including ALP, COL-1, OCN and Runx-2, inside the osteoblasts. As shown in Fig. 6(c), during the biodegradation of Zn0.8Li0.1Sr, $\rm Zn^{2+}$, $\rm Li^+$ and $\rm Sr^{2+}$ were released into the ambient marrow cavity. Low doses of these ions can increase the expression of Runx-2 gene [77]. The expression product (Runx-2 protein) can up-regulate the expression of ALP, COL-1 and OCN [42]. ALP and COL-1 are key participants in promoting the differentiation of osteoblasts and increasing the growth of new bone [78]. $\rm Zn^{2+}$ together with Runx-2 could up-regulate the expression of Osterix gene, whose expression product is OCN [79]. OCN is a key protein for the mineralization of bone matrix. Through these processes, Zn0.8Li0.1Sr and its biodegradation products promoted the activities of osteoblasts.

Except for promoting the activity of osteoblasts and inducing the expression of four critical genes, Zn^{2+} , Li^+ and Sr^{2+} play important roles in the procedure of bone remodeling. As shown in Fig. 6(d), the bone remodeling procedure consists of two parts: bone resorption by osteoclasts, and bone formation by osteoblasts [80]. For the bone resorption part, firstly hematopoietic stem cell (HSC) will differentiate into osteoclast precursor (Pre-OC), and then Pre-OCs will proliferate into osteoclasts [81]. For the bone formation part, firstly mesenchymal stem cell (MSC) will differentiate into osteoblast precursor (Pre-OB), and then Pre-OBs will proliferate into osteoblasts. Furthermore, when osteoblasts were embedded into bone matrix, they will grow numerous long

dendrite which could sense the mechanical stresses and maintain the optimal bone structure [82].

 ${\rm Zn}^{2+}$ can stimulate the bone formation and inhibit the bone resorption at the same time [83,84]. Through Wnt/ β -catenin pathway, Zn²⁺ can promote the differentiation and proliferation of osteoblasts [85]. And through NF-κB pathway, Zn²⁺ can accelerate the apoptosis of osteoclasts, thus reducing the bone resorption rate [86,87]. Li⁺ could promote the proliferation of osteoblasts mainly through the Wnt/β-catenin pathway [77,88–90], acting as inhibitor of GSK-3β and increasing expression of β -catenin. Sr^{2+} is well-known for its osteoporotic-bone-fracture-treating functions. Sr²⁺ has similar characters to Ca²⁺, and thus acting as an agonist of calcium-sensing receptor (CaSR) [91]. Sr²⁺ can promote bone formation and inhibit bone resorption mainly in three ways. Firstly, through the CaSR of MSC, Sr²⁺ can promote the differentiation and proliferation of osteoblasts. Secondly, together with Zn²⁺, Sr²⁺ can stimulate the NF-κB pathway and accelerate the apoptosis of osteoclasts. Thirdly, through the CaSR of osteoblasts, Sr²⁺ can increase the expression of osteoprotegerin (OPG) and reduce the expression of the RANK ligand (RANKL) [92–94]. RANKL is an expression product of osteoblasts and osteocytes [88], which would stimulate the receptor activator of nuclear factor-B (RANK) on the Pre-OCs. After the stimulation, Pre-OCs would proliferate into osteoclasts. OPG acts as an natural antagonist of RANKL. Through increasing the expression of OPG and reducing the expression of RANKL, Sr²⁺ can indirectly retard the proliferation of osteoclasts, and thus inhibiting the bone resorption procedure [82,88].

In this study, the mechanisms why Zn0.8Li0.1Sr could induce osteogenesis and therefore treat osteoporotic bone fractures were investigated both *in vitro* and *in vivo*. Firstly, the *in vitro* ALP tests and real-time PCR were employed to study the induction of osteogenesis in the MC3T3-E1 cells. Secondly, animal tests and further immunohistochemical analyses were conducted to reveal the induction of osteogenesis *in vivo*. The *in vitro* ALP tests (Fig. 4(a)(b)(d)(e)) shows that the expression of ALP in the Zn0.8Li0.1Sr was significantly higher than in the Zn0.8Li group. The real-time PCR results (Fig. 4(f)–(i)) show that Zn0.8Li0.1Sr induced higher expressions of all four genes being studied: ALP, COL-1, OCN and Runx-2, than the control groups.

As the immunohistochemical results of slices (Fig. 7(d)–(g)) obtained from the femur bone of OVX rats show, at 12 weeks, there were significantly higher expression of all four genes in the Z-12 group than in the T-12 group. In Z-12 group, the highest expression of four genes emerged in the collagen layer closest to the intramedullary nails. At 24 weeks, the previously grown collagen layer have largely transformed into osteoid and new bone tissue. The uniformly distributed trabeculae indicated a healthy growth status of the femur bone. As the EDS line scan results (Fig. 6(g)(h)) confirmed, the osteoid and new bone tissue were next close to the biodegradation products of Zn0.8Li0.1Sr intramedullary nail. It is reasonable to say that Zn0.8Li0.1Sr and its biodegradation products have made a great impact on the expression of these four osteogenesis-related genes in the femur bone of OVX rats. The X-ray scanning results, the explanted femur bones and the Micro-CT results (Fig. 5(a)-(c)) all confirmed that the femur bone grew better in the Zn0.8Li0.1Sr groups than in the pure Ti groups. The histological evaluations of organs (Fig. 8(a)), the ion concentrations of Zn²⁺, Li⁺ and Sr^{2+} (Fig. 8(b)) and the blood biochemistry analyses (Fig. 8(c)) all revealed that Zn0.8Li0.1Sr can serve as safely as pure Ti in vivo. In a word, as to biosafety, the Zn0.8Li0.1Sr performed as well as pure Ti. While as to osteogenesis-inducing, the Zn0.8Li0.1Sr obviously outperformed pure Ti. Through the biodegradation process and the synergic effects of Zn²⁺, Li⁺ and Sr²⁺, Zn0.8Li0.1Sr simultaneously promoted the bone formation and inhibited the bone resorption. As a result, Zn0.8Li0.1Sr significantly maintained bone mass (Fig. 5(d)), and successfully treated the osteoporotic bone fractures.

In this paper, the bio-compatibility and biodegradation behaviors of Zn0.8Li0.1Sr alloy was studied using OVX rats model. However, the information that could be conveyed from one paper is very limited. The

performances of biodegradable alloys were closely related to the surrounding environment and the bone metabolism. In addition, any changes in the buffering system, animal species and implantation position would greatly affect the alloys' biodegradation behaviors. To further illustrate the biological functions and biodegradation behaviors of ZnLiSr alloys, more researches using different models are still demanded.

5. Conclusion

In this paper, a brand-new biodegradable metal system, ZnLiSr, was developed and carefully investigated. Main conclusions can be drawn as followed:

- (1) ZnLiSr biodegradable metal system exhibits excellent comprehensive mechanical properties. In this system, Zn0.8Li0.1Sr exhibits the highest ultimate tensile strength (524.33 \pm 18.01 MPa), with a strength-ductility balance over 10 GPa%.
- (2) Zn0.8Li0.1Sr holds a similar biosafety level to pure Ti, while significantly superior osteogenesis-inducing and osteoporoticbone-fracture-treating effects than pure Ti. Zn0.8Li0.1Sr simultaneously promoted the bone formation and reduced the bone resorption through the bio-functions of Zn²⁺, Li⁺, and Sr²⁺, stimulating the expression of four critical genes (ALP, COL-1, OCN and Runx-2).
- (3) Zn0.8Li0.1Sr manifests mild and uniform degradation behaviors, with an *in vitro* degradation rate of $10.13 \pm 1.52 \ \mu m \ year^{-1}$.

In this paper, the employed means to study the Zn0.8Li0.1Sr alloy include mechanical tests, *in vitro* degradation tests, cell tests, and animal tests, etc. All these investigations verified that Zn0.8Li0.1Sr owns a trinity of osteoporotic-bone-fracture-treating effects, good biosafety as well as excellent mechanical properties, which would provide preferable choices for medical applications in the future.

Credit author statement

Zechuan Zhang: Conceptualization, Methodology, Investigation, Writing -original draft, Data curation. Bo Jia: Conceptualization, Methodology, Investigation, Writing -review &editing. Hongtao Yang: Conceptualization, Methodology, Investigation. Yu Han: Investigation. Qiang Wu: Investigation. Kerong Dai: Conceptualization, Methodology, Resources, Supervision, Project administration, Funding acquisition. Yufeng Zheng: Conceptualization, Methodology, Resources, Supervision, Writing -review &editing, Project administration, Funding acquisition.

Declaration of competing interest

The authors declare that they have no known competing financial interests or personal relationships that could have appeared to influence the work reported in this paper.

Acknowledgements

This work was supported by National Natural Science Foundation of China (Grant No. 51931001).

Appendix A. Supplementary data

Supplementary data to this article can be found online at https://doi.org/10.1016/j.biomaterials.2021.120905.

References

- [1] B.C. Lupsa, K. Insogna, Bone Health and Osteoporosis, Endocrinology and Metabolism Clinics of North America 44 (3) (2015) 517–530.
- [2] U. Nations, World Population Prospects 2019: Highlights, ST/ESA/SER.A/423), United Nations, New York, 2019.
- [3] L.A. Russell, Management of difficult osteoporosis, Best Pract. Res. Clin. Rheumatol. 32 (6) (2018) 835–847.
- [4] E. Seeman, T.J. Martin, Antiresorptive and anabolic agents in the prevention and reversal of bone fragility, Nat. Rev. Rheumatol. 15 (4) (2019) 225–236.
- [5] Y.F. Zheng, X.N. Gu, F. Witte, Biodegradable metals, Mater. Sci. Eng. R 77 (2014) 1–34.
- [6] P. Erne, M. Schier, T.J. Resink, The road to bioabsorbable stents: reaching clinical reality? Cardiovasc. Intervent. Radiol. 29 (1) (2006) 11–16.
- [7] R.B. Minkowitz, S. Bhadsavle, M. Walsh, K.A. Egol, Removal of painful orthopaedic implants after fracture union, J. Bone Joint Surg. 89 (9) (2007) 1906–1912.
- [8] J.C. Middleton, A.J. Tipton, Synthetic biodegradable polymers as orthopedic devices, Biomaterials 21 (23) (2000) 2335–2346.
- [9] S. Ray, U. Thormann, M. Eichelroth, M. Budak, C. Biehl, M. Rupp, U. Sommer, T. El Khassawna, F.I. Alagboso, M. Kampschulte, M. Rohnke, A. Henss, K. Peppler, V. Linke, P. Quadbeck, A. Voigt, F. Stenger, D. Karl, R. Schnettler, C. Heiss, K. S. Lips, V. Alt, Strontium and bisphosphonate coated iron foam scaffolds for osteoporotic fracture defect healing, Biomaterials 157 (2018) 1–16.
- [10] G. Song, Control of biodegradation of biocompatable magnesium alloys, Corrosion Sci. 49 (2007) 1696–1701.
- [11] D. Vojtech, J. Kubasek, J. Serak, P. Novak, Mechanical and corrosion properties of newly developed biodegradable Zn-based alloys for bone fixation, Acta Biomater. 7 (2011) 3515–3522.
- [12] H.J. Seo, Y.E. Cho, T. Kim, H.I. Shin, I.S. Kwun, Zinc may increase bone formation through stimulating cell proliferation, alkaline phosphatase activity and collagen synthesis in osteoblastic MC3T3-E1 cells, Nutrit. Res. Pract. 4 (5) (2010) 356–361.
- [13] Y. Liu, Y. Zheng, X.-H. Chen, J.-A. Yang, H. Pan, D. Chen, L. Wang, J. Zhang, D. Zhu, S. Wu, K.W.K. Yeung, R.-C. Zeng, Y. Han, S. Guan, Fundamental theory of biodegradable metals-definition, criteria, and design, Adv. Funct. Mater. (2019) 1805402.
- [14] J. Kubasek, D. Vojtech, E. Jablonska, I. Pospisilova, J. Lipov, T. Ruml, Structure, mechanical characteristics and in vitro degradation, cytotoxicity, genotoxicity and mutagenicity of novel biodegradable Zn-Mg alloys, Mater. Sci. Eng. C 58 (2016) 24-35.
- [15] S. Zhao, C.T. McNamara, P.K. Bowen, N. Verhun, J.P. Braykovich, J. Goldman, J. W. Drelich, Structural characteristics and in vitro biodegradation of a novel Zn-Li alloy prepared by induction melting and hot rolling, Metall. Mater. Trans. 48 (3) (2017) 1204–1215.
- [16] Z. Li, Z.-Z. Shi, Y. Hao, H.-F. Li, X.-F. Liu, A.A. Volinsky, H.-J. Zhang, L.-N. Wang, High-performance hot-warm rolled Zn-0.8Li alloy with nano-sized metastable precipitates and sub-micron grains for biodegradable stents, J. Mater. Sci. Technol. 35 (11) (2019) 2618–2624.
- [17] H. Yang, B. Jia, Z. Zhang, X. Qu, G. Li, W. Lin, D. Zhu, K. Dai, Y. Zheng, Alloying design of biodegradable zinc as promising bone implants for load-bearing applications, Nat. Commun. 11 (1) (2020) 401.
- [18] J. Venezuela, M.S. Dargusch, The influence of alloying and fabrication techniques on the mechanical properties, biodegradability and biocompatibility of zinc: a comprehensive review, Acta Biomater. 87 (2019) 1–40.
- [19] H.F. Li, X.H. Xie, Y.F. Zheng, Y. Cong, F.Y. Zhou, K.J. Qiu, X. Wang, S.H. Chen, L. Huang, L. Tian, L. Qin, Development of biodegradable Zn-1X binary alloys with nutrient alloying elements Mg, Ca and Sr, Sci. Rep. 5 (2015) 10719.
- [20] D. Zhu, I. Cockerill, Y. Su, Z. Zhang, J. Fu, K.W. Lee, J. Ma, C. Okpokwasili, L. Tang, Y. Zheng, Y.X. Qin, Y. Wang, Mechanical strength, biodegradation, and in vitro and in vivo biocompatibility of Zn biomaterials, ACS Appl. Mater. Interfaces 11 (7) (2019) 6809–6819.
- [21] B. Jia, H. Yang, Y. Han, Z. Zhang, X. Qu, Y. Zhuang, Q. Wu, Y. Zheng, K. Dai, In vitro and in vivo studies of Zn-Mn biodegradable metals designed for orthopedic applications, Acta Biomater. 108 (2020) 358–372.
- [22] M. Lolov, N. Djulgerov, S. Gyurov, Study of the peculiarities of the Zn-Mn phase diagram and their effect on the superplastic behavior of fine-grained Zn-Mn alloys, J. Mater. Eng. Perform. 25 (9) (2016) 3838–3844.
- [23] Y.X. Yin, C. Zhou, Y.P. Shi, Z.Z. Shi, T.H. Lu, Y. Hao, C.H. Liu, X. Wang, H.J. Zhang, L.N. Wang, Hemocompatibility of biodegradable Zn-0.8wt% (Cu, Mn, Li) alloys, Mater. Sci. Eng. C 104 (2019) 109896.
- [24] A. Kafri, S. Ovadia, G. Yosafovich-Doitch, E. Aghion, In vivo performances of pure Zn and Zn-Fe alloy as biodegradable implants, J. Mater. Sci. Mater. Med. 29 (7) (2018) 94.
- [25] J. Niu, Z. Tang, H. Huang, J. Pei, H. Zhang, G. Yuan, W. Ding, Research on a Zn-Cu alloy as a biodegradable material for potential vascular stents application, Mater. Sci. Eng. C 69 (2016) 407–413.
- [26] Z. Tang, J. Niu, H. Huang, H. Zhang, J. Pei, J. Ou, G. Yuan, Potential biodegradable Zn-Cu binary alloys developed for cardiovascular implant applications, J. Mech. Behav. Biomed. Mater. 72 (2017) 182–191.
- [27] K.B. Törne, F.A. Khan, A. Örnberg, J. Weissenrieder, Zn-Mg and Zn-Ag degradation mechanism under biologically relevant conditions, Surface Innov. (2017) 1–41.
- [28] M. Sikora-Jasinska, E. Mostaed, A. Mostaed, R. Beanland, D. Mantovani, M. Vedani, Fabrication, mechanical properties and in vitro degradation behavior of newly developed ZnAg alloys for degradable implant applications, Mater. Sci. Eng. C 77 (2017) 1170–1181.
- [29] U. Thormann, S. Ray, U. Sommer, T. Elkhassawna, T. Rehling, M. Hundgeburth, A. Henss, M. Rohnke, J. Janek, K.S. Lips, C. Heiss, G. Schlewitz, G. Szalay,

- M. Schumacher, M. Gelinsky, R. Schnettler, V. Alt, Bone formation induced by strontium modified calcium phosphate cement in critical-size metaphyseal fracture defects in ovariectomized rats, Biomaterials 34 (34) (2013) 8589–8598.
- [30] E. Gentleman, Y.C. Fredholm, G. Jell, N. Lotfibakhshaiesh, M.D. O'Donnell, R. G. Hill, M.M. Stevens, The effects of strontium-substituted bioactive glasses on osteoblasts and osteoclasts in vitro, Biomaterials 31 (14) (2010) 3949–3956.
- [31] J. Lao, E. Jallot, J.-M. Nedelec, Strontium-delivering glasses with enhanced bioactivity: a new biomaterial for antiosteoporotic applications? Chem. Mater. 20 (2008) 4969–4973.
- [32] Z.Y. Li, W.M. Lam, C. Yang, B. Xu, G.X. Ni, S.A. Abbah, K.M. Cheung, K.D. Luk, W. Uu, Chemical composition, crystal size and lattice structural changes after incorporation of strontium into biomimetic apatite, Biomaterials 28 (7) (2007) 1452–1460.
- [33] O.Z. Andersen, V. Offermanns, M. Sillassen, K.P. Almtoft, I.H. Andersen, S. Sorensen, C.S. Jeppesen, D.C. Kraft, J. Bottiger, M. Rasse, F. Kloss, M. Foss, Accelerated bone ingrowth by local delivery of strontium from surface functionalized titanium implants, Biomaterials 34 (24) (2013) 5883–5890.
- [34] X.N. Gu, X.H. Xie, N. Li, Y.F. Zheng, L. Qin, In vitro and in vivo studies on a Mg-Sr binary alloy system developed as a new kind of biodegradable metal, Acta Biomater. 8 (6) (2012) 2360–2374.
- [35] M.-C. Zhao, Y.-C. Zhao, D.-F. Yin, S. Wang, Y.-M. Shangguan, C. Liu, L.-L. Tan, C.-J. Shuai, K. Yang, A. Atrens, Biodegradation behavior of coated as-extruded Mg-Sr alloy in simulated body fluid, Acta Metall. Sin. 32 (10) (2019) 1195–1206.
- [36] W. Li, X. Liu, Y. Zheng, W. Wang, W. Qiao, K.W.K. Yeung, K.M.C. Cheung, S. Guan, O.B. Kulyasova, R.Z. Valiev, In vitro and in vivo studies on ultrafine-grained biodegradable pure Mg, Mg-Ca alloy and Mg-Sr alloy processed by high-pressure torsion, Biomater. Sci. 8 (18) (2020) 5071–5087.
- [37] T. Kokubo, H. Takadama, How useful is SBF in predicting in vivo bone bioactivity? Biomaterials 27 (15) (2006) 2907–2915.
- [38] X. Liu, H. Yang, P. Xiong, W. Li, H.-H. Huang, Y. Zheng, Comparative studies of Tris-HCl, HEPES and NaHCO3/CO2 buffer systems on the biodegradation behaviour of pure Zn in NaCl and SBF solutions, Corrosion Sci. 157 (2019) 205–219.
- [39] H.M. Abuohashish, M.M. Ahmed, S.S. Al-Rejaie, K.E. Eltahir, The antidepressant bupropion exerts alleviating properties in an ovariectomized osteoporotic rat model, Acta Pharmacol. Sin. 36 (2) (2015) 209–220.
- [40] T.J. Wronski, P.L. Lowry, C.C. Walsh, L.A. Ignaszewski, Skeletal alterations in ovariectomized rats, Calcif. Tissue Int. 37 (1985) 324–328.
- [41] W. Huang, S. Yang, J. Shao, Y. Li, Signaling and transcriptional regulation in osteoblast commitment and differentiation, Front. Biosci. 12 (2007) 3068–3092.
- [42] M. Bruderer, R.G. Richards, M. Alini, M.J. Stoddart, Role and regulation of RUNX2 in osteogenesis, Eur. Cell. Mater. 28 (2014) 269–286.
- [43] I.C. Santos, G.S. Gazelle, L.A. Rocha, J.M. Tavares, Medical device specificities: opportunities for a dedicated product development methodology, Expet Rev. Med. Dev. 9 (3) (2012) 299–311.
- [44] J.W. Lee, H.S. Han, K.J. Han, J. Park, H. Jeon, M.R. Ok, H.K. Seok, J.P. Ahn, K. E. Lee, D.H. Lee, S.J. Yang, S.Y. Cho, P.R. Cha, H. Kwon, T.H. Nam, J.H. Han, H. J. Rho, K.S. Lee, Y.C. Kim, D. Mantovani, Long-term clinical study and multiscale analysis of in vivo biodegradation mechanism of Mg alloy, Proceed. Natl. Acad. Sci. U.S.A. 113 (3) (2016) 716–721.
- [45] H. Windhagen, K. Radtke, A. Weizbauer, J. Diekmann, Y. Noll, U. Kreimeyer, R. Schavan, C. Stukenborg-Colsman, H. Waizy, Biodegradable magnesium-based screw clinically equivalent to titanium screw in hallux valgus surgery: short term results of the first prospective, randomized, controlled clinical pilot study, Biomed. Eng. Online 12 (2013), 62-62.
- [46] Y. Wei, Y. Li, L. Zhu, Y. Liu, X. Lei, G. Wang, Y. Wu, Z. Mi, J. Liu, H. Wang, H. Gao, Evading the strength-ductility trade-off dilemma in steel through gradient hierarchical nanotwins. Nat. Commun. 5 (2014) 3580.
- [47] R.O. Ritchie, The conflicts between strength and toughness, Nat. Mater. 10 (11) (2011) 817–822.
- [48] T. Kong, B.J. Kwak, J. Kim, J.H. Lee, S.H. Park, J.H. Kim, Y.H. Moon, H.S. Yoon, T. Lee, Tailoring strength-ductility balance of caliber-rolled AZ31 Mg alloy through subsequent annealing, J. Magnesium Alloys 8 (1) (2020) 163–171.
- [49] J. She, S.B. Zhou, P. Peng, A.T. Tang, Y. Wang, H.C. Pan, C.L. Yang, F.S. Pan, Improvement of strength-ductility balance by Mn addition in Mg–Ca extruded alloy, Mater. Sci. Eng., A 772 (2020) 138796.
- [50] Z. Li, X. Gu, S. Lou, Y. Zheng, The development of binary Mg-Ca alloys for use as biodegradable materials within bone, Biomaterials 29 (10) (2008) 1329–1344.
- [51] Y. Liu, Y. Wu, D. Bian, S. Gao, S. Leeflang, H. Guo, Y. Zheng, J. Zhou, Study on the Mg-Li-Zn ternary alloy system with improved mechanical properties, good degradation performance and different responses to cells, Acta Biomater. 62 (2017) 418–433.
- [52] D. Bian, W. Zhou, J. Deng, Y. Liu, W. Li, X. Chu, P. Xiu, H. Cai, Y. Kou, B. Jiang, Y. Zheng, Development of magnesium-based biodegradable metals with dietary trace element germanium as orthopaedic implant applications, Acta Biomater. 64 (2017) 421–436.
- [53] M.I. Sabir, X. Xu, L. Li, A review on biodegradable polymeric materials for bone tissue engineering applications, J. Mater. Sci. 44 (21) (2009) 5713–5724.
- [54] J. Liu, D. Bian, Y. Zheng, X. Chu, Y. Lin, M. Wang, Z. Lin, M. Li, Y. Zhang, S. Guan, Comparative in vitro study on binary Mg-RE (Sc, Y, La, Ce, Pr, Nd, Sm, Eu, Gd, Tb, Dy, Ho, Er, Tm, Yb and Lu) alloy systems, Acta Biomater. 102 (2020) 508–528.
- [55] H. Hermawan, D. Dube, D. Mantovani, Developments in metallic biodegradable stents, Acta Biomater. 6 (5) (2010) 1693–1697.
- [56] P. Han, P. Cheng, S. Zhang, C. Zhao, J. Ni, Y. Zhang, W. Zhong, P. Hou, X. Zhang, Y. Zheng, Y. Chai, In vitro and in vivo studies on the degradation of high-purity Mg

- (99.99wt.%) screw with femoral intracondylar fractured rabbit model, Biomaterials 64 (2015) 57–69.
- [57] E. Mostaed, M. Sikora-Jasinska, A. Mostaed, S. Loffredo, A.G. Demir, B. Previtali, D. Mantovani, R. Beanland, M. Vedani, Novel Zn-based alloys for biodegradable stent applications: design, development and in vitro degradation, J. Mech. Behav. Biomed. Mater. 60 (2016) 581–602.
- [58] E. Mostaed, M. Sikora-Jasinska, J.W. Drelich, M. Vedani, Zinc-based alloys for degradable vascular stent applications, Acta Biomater. 71 (15) (2018) 1–23.
- [59] X. Liu, J. Sun, F. Zhou, Y. Yang, R. Chang, K. Qiu, Z. Pu, L. Li, Y. Zheng, Microalloying with Mn in Zn–Mg alloy for future biodegradable metals application, Mater. Des. 94 (2016) 95–104.
- [60] Z.-Z. Shi, J. Yu, X.-F. Liu, L.-N. Wang, Fabrication and characterization of novel biodegradable Zn-Mn-Cu alloys, J. Mater. Sci. Technol. 34 (6) (2017) 1008–1015.
- [61] X. Liu, J. Sun, Y. Yang, F. Zhou, Z. Pu, L. Li, Y. Zheng, Microstructure, mechanical properties, in vitro degradation behavior and hemocompatibility of novel Zn–Mg–Sr alloys as biodegradable metals, Mater. Lett. 162 (2016) 242–245.
- [62] F. Zivic, S. Affatato, M. Trajanovic, M. Schnabelrauch, N. Grujovic, K.L. Choy, Biomaterials in Clinical Practice, Springer, 2017.
- [63] L.-Q. Wang, Y.-P. Ren, S.-N. Sun, H. Zhao, S. Li, G.-W. Qin, Microstructure, mechanical properties and fracture behavior of as-extruded Zn–Mg binary alloys, Acta Metall. Sin. 30 (10) (2017) 931–940.
- [64] G. Li, H. Yang, Y. Zheng, X.H. Chen, J.A. Yang, D. Zhu, L. Ruan, K. Takashima, Challenges in the use of zinc and its alloys as biodegradable metals: perspective from biomechanical compatibility, Acta Biomater. 97 (2019) 23–45.
- [65] A. Kafri, S. Ovadia, J. Goldman, J. Drelich, E. Aghion, The suitability of Zn-1.3%Fe alloy as a biodegradable implant, Mater. Metals 8 (3) (2018) 153–167.
- [66] W. Yuan, D. Xia, Y. Zheng, X. Liu, S. Wu, B. Li, Y. Han, Z. Jia, D. Zhu, L. Ruan, K. Takashima, Y. Liu, Y. Zhou, Controllable biodegradation and enhanced osseointegration of ZrO2-nanofilm coated Zn-Li alloy: in vitro and in vivo studies, Acta Biomater. 105 (2020) 290–303.
- [67] H. Guo, D. Xia, Y. Zheng, Y. Zhu, Y. Liu, Y. Zhou, A pure zinc membrane with degradability and osteogenesis promotion for guided bone regeneration: in vitro and in vivo studies, Acta Biomater. 106 (2020) 396–409.
- [68] H.-S. Han, S. Loffredo, I. Jun, J. Edwards, Y.-C. Kim, H.-K. Seok, F. Witte, D. Mantovani, S. Glyn-Jones, Current status and outlook on the clinical translation of biodegradable metals, Mater. Today 23 (2019) 57–71.
- [69] B. Liu, Y.F. Zheng, L. Ruan, In vitro investigation of Fe30Mn6Si shape memory alloy as potential biodegradable metallic material, Mater. Lett. 65 (3) (2011) 540–543.
- [70] B. Liu, Y.F. Zheng, Effects of alloying elements (Mn, Co, Al, W, Sn, B, C and S) on biodegradability and in vitro biocompatibility of pure iron, Acta Biomater. 7 (3) (2011) 1407–1420.
- [71] M.H. Elahinia, M. Hashemi, M. Tabesh, S.B. Bhaduri, Manufacturing and processing of NiTi implants: a review, Prog. Mater. Sci. 57 (5) (2012) 911–946.
- [72] M. Geetha, A.K. Singh, R. Asokamani, A.K. Gogia, Ti based biomaterials, the ultimate choice for orthopaedic implants – a review, Prog. Mater. Sci. 54 (3) (2009) 397–425.
- [73] J.C. Frame, P.-Y. Rohan, L. Corté, R. Allena, Optimal bone structure is dependent on the interplay between mechanics and cellular activities, Mech. Res. Commun. 92 (2018) 43–48.
- [74] Y. Yang, Q. Yu, Z. He, J. Ma, J. Qin, Investigation on failure mechanism of stiffened plates with pitting corrosion under uniaxial compression, Appl. Ocean Res. 102 (2020) 102318.
- [75] N. Oshibe, E. Marukawa, T. Yoda, H. Harada, Degradation and interaction with bone of magnesium alloy WE43 implants: a long-term follow-up in vivo rat tibia study, J. Biomater. Appl. 33 (9) (2019) 1157–1167.

- [76] S.H. Byun, H.K. Lim, K.H. Cheon, S.M. Lee, H.E. Kim, J.H. Lee, Biodegradable magnesium alloy (WE43) in bone-fixation plate and screw, J. Biomed. Mater. Res. B Appl. Biomater. 108 (6) (2020) 2505–2512.
- [77] A.T. Posch, J.F. de Avellar-Pinto, F.S. Malta, L.M. Marins, L.N. Teixeira, D. C. Peruzzo, E.F. Martinez, J.T. Clemente-Napimoga, P.M. Duarte, M.H. Napimoga, Lithium chloride improves bone filling around implants placed in estrogen-deficient rats, Arch. Oral Biol. 111 (2020) 104644.
- [78] G. Kirkham, S. Cartmell, Genes and proteins involved in the regulation of osteogenesis, Top. Tissue Eng. 3 (2007) 1–22.
- [79] K. Nakashima, X. Zhou, G. Kunkel, Z. Zhang, J.M. Deng, R.R. Behringer, B. De Crombrugghe, The novel zinc finger-containing transcription factor Osterix is required for osteoblast differentiation and bone formation, Cell 108 (1) (2002) 17–29
- [80] E. Canalis, A. Giustina, J.P. Bilezikian, Mechanisms of anabolic therapies for osteoporosis, N. Engl. J. Med. 357 (9) (2007) 905–916.
- [81] N. Maximova, F. Zennaro, M. Gregori, G. Boz, D. Zanon, G. Mbalaviele, Hematopoietic stem cell transplantation-induced bone remodeling in autosomal recessive osteopetrosis: interaction between skeleton and hematopoietic and sensory nervous systems, Bone 130 (2020) 115144.
- [82] A.I. Gogakos, M.S. Cheung, J.H.D. Bassett, G.R. Williams, Bone signaling pathways and treatment of osteoporosis, Expet Rev. Endocrinol. Metabol. 4 (6) (2009) 639-650
- [83] N.M. Lowe, N.M. Lowe, W.D. Fraser, M.J. Jackson, Is there a potential therapeutic value of copper and zinc for osteoporosis? Proc. Nutr. Soc. 61 (2) (2002) 181–185.
- [84] J. Zheng, X. Mao, J. Ling, Q. He, J. Quan, Low serum levels of zinc, copper, and iron as risk factors for osteoporosis: a meta-analysis, Biol. Trace Elem. Res. 160 (1) (2014) 15–23.
- [85] M. Jimenez, C. Abradelo, J. San Roman, L. Rojo, Bibliographic review on the state of the art of strontium and zinc based regenerative therapies. Recent developments and clinical applications, J. Mater. Chem. B 7 (12) (2019) 1974–1985.
- [86] N.S. Soysa, N. Alles, NF-kappaB functions in osteoclasts, Biochem. Biophys. Res. Commun. 378 (1) (2009) 1–5.
- [87] A. Gür, L. Çolpan, K. Nas, R. Çevik, J. Saraç, F. Erdoan, M.Z. Düz, The role of trace minerals in the pathogenesis of postmenopausal osteoporosis and a new effect of calcitonin, J. Bone Miner. Metabol. 20 (1) (2002) 39–43.
- [88] S.C. Manolagas, Wnt signaling and osteoporosis, Maturitas 78 (3) (2014) 233-237.
- [89] L. Li, X. Peng, Y. Qin, R. Wang, J. Tang, X. Cui, T. Wang, W. Liu, H. Pan, B. Li, Acceleration of bone regeneration by activating Wnt/beta-catenin signalling pathway via lithium released from lithium chloride/calcium phosphate cement in osteoporosis, Sci. Rep. 7 (2017) 45204.
- [90] Y. Jin, L. Xu, X. Hu, S. Liao, J.L. Pathak, J. Liu, Lithium chloride enhances bone regeneration and implant osseointegration in osteoporotic conditions, J. Bone Miner. Metabol. 35 (5) (2017) 497–503.
- [91] A.S. Hurtel-Lemaire, R. Mentaverri, A. Caudrillier, F. Cournarie, A. Wattel, S. Kamel, E.F. Terwilliger, E.M. Brown, M. Brazier, The calcium-sensing receptor is involved in strontium ranelate-induced osteoclast apoptosis. New insights into the associated signaling pathways, J. Biol. Chem. 284 (1) (2009) 575–584.
- [92] S.D. Bain, C. Jerome, V. Shen, I. Dupin-Roger, P. Ammann, Strontium ranelate improves bone strength in ovariectomized rat by positively influencing bone resistance determinants, Osteoporos. Int. 20 (8) (2009) 1417–1428.
- [93] C. Ehret, R. Aid-Launais, T. Sagardoy, R. Siadous, R. Bareille, S. Rey, S. Pechev, L. Etienne, J. Kalisky, E. de Mones, D. Letourneur, J. Amedee Vilamitjana, Strontium-doped hydroxyapatite polysaccharide materials effect on ectopic bone formation, PloS One 12 (9) (2017), e0184663.
- [94] T.C. Brennan, M.S. Rybchyn, W. Green, S. Atwa, A.D. Conigrave, R.S. Mason, Osteoblasts play key roles in the mechanisms of action of strontium ranelate, Br. J. Pharmacol. 157 (7) (2009) 1291–1300.